ABSTRACT

A 2007 Aircraft-based Study of Plumes from Biomass Burning Origin from Mexico and Central America Advected over South Texas and the Western Gulf of Mexico

Sergio L. Alvarez, I.M.E.S.

Mentor: Maxwell E. Shauck, Ph.D.

Biomass burning is the burning of living and dead vegetation which includes grasslands, forests, and agricultural lands (Levin, 1998). It is a global phenomenon and serves a multitude of purposes such as clearing of forests and brushland for agricultural use; control of weeds; production of charcoal; and energy production for cooking and heating (Crutzen and Andreae, 1990). The Baylor Institute for Air Science (BIAS) equipped an aircraft to measure trace gases and aerosols during two science flights in the south Texas region. One science flight was flown to collect "background" continental and marine layer air data and the other to collect data in biomass-burning smoke plumes from Mexico and Central American countries. Measurements were taken in the geographic region along the US-Mexico Border and adjacent area over the western Gulf of Mexico. Results of this study indicate that individual smoke plumes may occur episodically over the Texas border region to Mexico under prevailing southeasterly wind directions. The origin of these plumes may be diverse ranging from individual local fire emissions to medium range transport of biomass burning.

A 2007 Aircraft-based Study of Plumes from Biomass Burning Origin from Mexico and Central America Advected over South Texas and the Western Gulf of Mexico

by

Sergio L. Alvarez, B.S.

A Thesis

Approved by the Institute for Air Science

_____
Maxwell E. Shauck, Ph.D., Chairperson

Submitted to the Graduate Faculty of
Baylor University in Partial Fulfillment of the
Requirements for the Degree
of
International Master in Environmental Sciences

Approved by the Thesis Committee

_____
Maxwell E. Shauck, Ph.D., Chairperson

_____
Larry W. Olson, Ph.D., Chairperson

_____
Joseph D. White, Ph.D.

Accepted by the Graduate School
May 2009

_____
J. Larry Lyon, Ph.D., Dean

Page bearing signatures is kept on file in the Graduate Office

TABLE OF CONTENTS

LIST OF FIGURES

LIST OF TABLES

ACKNOWLEDGMENTS

The author gratefully acknowledges the NOAA Air Resources Laboratory (ARL) for the provision of the HYSPLIT transport and dispersion model and/or READY website (http://www.arl.noaa.gov/ready.html) used in this publication. In addition, the author acknowledges and thanks the Environmental Protection Agency (EPA), Zapata County, University of Houston and Baylor University for the use of the data.

ABBREVIATIONS

AIMMS-20	Aircraft-Integrated Meteorological Measurement System
BIAS	Baylor Institute for Air Science
Ca^{+}	Calcium ion
C	Carbon
CBL	Convective Boundary Layer
$CHOO^{-}$	Formate ion
CH_3Cl	Methyl chloride
$(CH_3COO)^{-}$	Acetate
CH_3CN	Acetonitrile
CH_4	Methane
C_2H_2	Acetylene
Cl^{-}	Chloride ion
C_3H_8	Propane
CO	Carbon Monoxide
CO_2	Carbon Dioxide
EPA	Environmental Protection Agency
ft	Feet
GC	Gas Chromatography
GOES	Geostationary Operational Environmental Satellites
HNO_3	Nitric acid

HYSPLIT	Hybrid Single Particle Lagrangian Integrated Trajectory Model
IC	Ion Chromatography
K^+	Potassium ion
m s^{-1}	meter per second
Mg^+	Magnesium ion
mm	milimeter
Lb	Pound
L	Liter
MODIS	MODerate resolution Imaging Spectrometer
MSL	Mean Sea Level
Na^+	Sodium ion
NAAPS	Navy Aerosol Analysis Prediction System
NAAQS	National Ambient Air Quality Standards
NCAR	National Center for Atmospheric Research
nm	nautical miles, also used as nanometers
NESDIS	National Environmental Satellite, Data, and Information Service
NIST	National Institute of Standards and Technology
NMHC	Non-Methane Hydrocarbons
NIST	National Institute of Standards and Technology
NO_3^-	Nitrate ion
NO_2	Nitrogen Dioxide
NOAA	National Oceanic and Atmospheric Administration

NOy	Reactive nitrogen
NH_4^+	Ammonium ion
NO	Nitric Oxide
NO_2	Nitrogen Dioxide
$(COO^-)_2$	Oxalate ion
NOx	Nitric Oxide and Nitrogen Dioxide
PALMS	Particle Analysis Laser Mass-Spectrometry
O_3	Ozone
SO_2	Sulfur Dioxide
SO_4^{2-}	Sulfate ion
TOMS	Total Ozone Mapping Spectrometer
UK NPL	United Kingdom National Physical Laboratory
UNC	University of New Hampshire
US	United States
VOC	Volatile Organic Compounds
VUV	Vacuum Ultraviolet

CHAPTER ONE

Introduction

Biomass burning is the burning of living and dead vegetation which includes grasslands, forests, and agricultural lands (Levin, 1998). It is a global phenomenon and serves a multitude of purposes such as clearing of forests and brushland for agricultural use; control of pests, insects, and weeds; prevention of litter accumulation to preserve pasturelands; nutrient mobilization; game hunting; production of charcoal for industrial use; energy production for cooking and heating; communication and transport; and various religious and aesthetic reasons (Crutzen and Andreae, 1990).

The earliest direct evidence for use of fire by hominids as a tool is 1 to 1.5 millions years ago (e.g., Brain and Sillen, 1988). However, natural fires have occurred since the evolution of plants 350 to 400 million years ago (e.g., Griffin and Goldberg, 1979). They were caused by lightning and volcanic lava efflux (Lobert et al, 1999). In recent decades, a temporal development of anthropogenic-induced fires has increased and is expected to continue (Rokjin et al, 2007). For example, in the Western US, Westerling et al. (2006) reports an increase in large fires since the 1970's, linked to increasing spring and summer temperatures. Today, fires are almost entirely anthropogenic (Trentmann, 2003). However in some regions of the world where boreal forests and savannas exist, natural wildfires play a significant role occurring every 3 to 5 years and some tens of years, respectively (Andreae, 1991, 1993; Andreae and Merlet, 2001, as cited in Trentman et al, 2003). It is estimated that more than 30% of the tropical biomass is

burned during savanna fires (e.g. Andreae, 1991), the largest single contribution to the annual, global biomass burning emission (Dwyer et al, 2000).

Furthermore, the majority of biomass burning occurs in the tropics during the dry season (Dwyer et al, 1998, Fearnside, 1990). For example, Central American biomass burning in the Yucatan Peninsula and southern Mexico typically occurs during March-May in the tropical dry season and ends in early June due to the beginning of the rainy season (Crutzen et al, 1979). In fact, past studies have documented during that time frame the transboundary pollutant effects in the US from biomass burning in Mexico and Central American (Peppler et al., 2000; Gebhart et al., 2001; Kreidenweis et al., 2001; de Gouw et al., 2003; Wang et al., 2006).

In addition, a region that often gets overlooked by extreme biomass burning events in Central America is northeastern Mexico which has been characterized as having >70% of its wildfires during the months of April and May (Mendoza et al, 2005). Just as Central America, the region has varying intensities (i.e., Spring 1998 severe and Spring 2006 light) of biomass burning from year to year and also occurs during the dry season. However it remains a re-occurring seasonal event in both regions (i.e., Central America and northern Mexico) within the April-May time frame. Satellite imagery data (i.e., visible and aerosol) from GOES (Geostationary Operational Environmental Satellite), TOMS (Total Ozone Mapping Spectrometer) and MODIS (MODerate resolution Imaging Spectrometer) has helped immensely in determining the origin and spatial extent of plumes from biomass burning (Hsu, et al, 1996, Hutchinson, 2003). In addition, direct measurements of trace gases and aerosols (including molecular markers) in ambient air have advanced the science used to determine the contribution of biomass burning to air

pollution. (e.g., Goode et al, 2000, de Gouw et al., 2003, Fraser et al., 2003) For example, molecular marker levoglucosan is used to track emissions from wood combustion (Simoneit et al., 1999; Fraser et al, 2004; Simpson et al, 2004) and acetonitrile is used as an indicator of biomass burning emissions (Holzinger et al., 1999; de Gouw et al, 2003; Sanhueza et al., 2003). Finally, these methods have made it possible to use emission factors and speciation profiles which can be used in modeling and source apportionment studies (Mendoza et al, 2005).

The implications of biomass burning are numerous and have been the focus of ongoing discussions within the scientific community. Mendoza et al (2005) writes, "The contribution of wildfires to the total emission of air pollution in Mexico is not well understood, nor the potential impact of those emissions in the air quality of the country and abroad." Biomass burning is a major source of atmospheric pollutants (e.g., Crutzen et al., 1979; Crutzen and Andreae, 1990; Andreae and Merlet, 2001, as cited in Keene et al, 2006) that significantly affect atmospheric and biogeochemical cycles on a regional and global scale (Keene et al, 2006). For instance, it has been suggested the buildup of carbon monoxide (CO) and methane (CH_4), i.e., primary pollutants from biomass burning, in the atmosphere may decrease hydroxide radical (OH), thereby decreasing the oxidizing capacity of the atmosphere (Crutzen et al, 1990).

Because of studies carried out in various locations worldwide, it is known that biomass burning produces a variety of chemical species (e.g. Trentmann et al., 2003; Hudson et al., 2004) and can be distinguished from other anthropogenic sources (Tang et al., 2003; de Gouw et al., 2004). For example, de Gouw et al (2004) use the ratio of measured acetylene (C_2H_2) to measured propane (C_3H_8), the percentage of particles

measured by particle analysis by laser mass spectrometry (PALMS) instrument that were attributed to biomass burning based on their carbon (C) and potassium (K) content, acetonitrile (CH_3CN) and methyl chloride (CH_3Cl). In this study an attempt will be made to use ratios between NMHCs (Non Methane Hydrocarbons) and CO, ratios between filter species (anions and cations) and single species such as K and oxalate to determine chemical signatures from biomass burning. Thus, the motivation and goal of the work presented here is to examine selected science flights which were performed by the Baylor Institute for Air Science during the 2007 biomass burning season (spring) for Zapata County. These flights were targeted at potential biomass burning plumes originating from Central America and southern Mexico which eventually may impact the South Texas region and beyond under southerly wind flow conditions which are typical for this time of the year. Measurements were made over South Texas, the geographic region along the US-Mexico Border. The region encompassed Zapata, Texas, and extended to the western Gulf of Mexico. In this work two science flights, one without plumes containing biomass-burning chemical signatures and the other with them will be presented and discussed in detail.

CHAPTER TWO

Methods

Description of Region of Study

Zapata County, including the mid-to-lower Rio Grande Valley region (McAllen, to Brownsville, Texas) experiences poor air quality, particularly in the late spring (Alvarez et al, 2008). The lower Rio Grande Valley is the tip of Texas and includes a four-county area, i.e., Cameron, Hidalgo, Starr and Willacy Counties. The population is 1.14 million and has increased drastically over the last decades (62.5% between 1990 and 2006). It is also the center of the region most recently named Rioplex, which includes Northern Mexico border cities between Matamoros and Cuidad Mier (McAllen Chamber of Commerce, 2008). As a consequence, the total population of that region is well over 3.9 million and thus also contributes to local air pollutant emissions.

On the south side of the border, three major cities, Matamoros, Rio Bravo and Reynosa, are where the majority of the maquiladora industry is located. Maquiladoras are defined as factories that import materials and equipment on a duty-free basis for assembly or manufacturing, and then re-export the assembled product (Wikipedia, 2004). In addition, they are considered point sources that likely contribute to the local air quality and potentially regional air quality as well. Figure 1 illustrates a regional view of South Texas and indicates the city of Zapata, with circle, which is also the location of the Zapata County airport where the aircraft was temporarily based. In addition, it shows the geographic area the aircraft flew over, which includes a swath of geographical area that is parallel to the US-Mexico Border, just north of the Rio Grande River, from the city of

Zapata to the Western Gulf of Mexico. The bi-national metropolitan area of Rioplex is also indicated with a black-dashed rectangle.

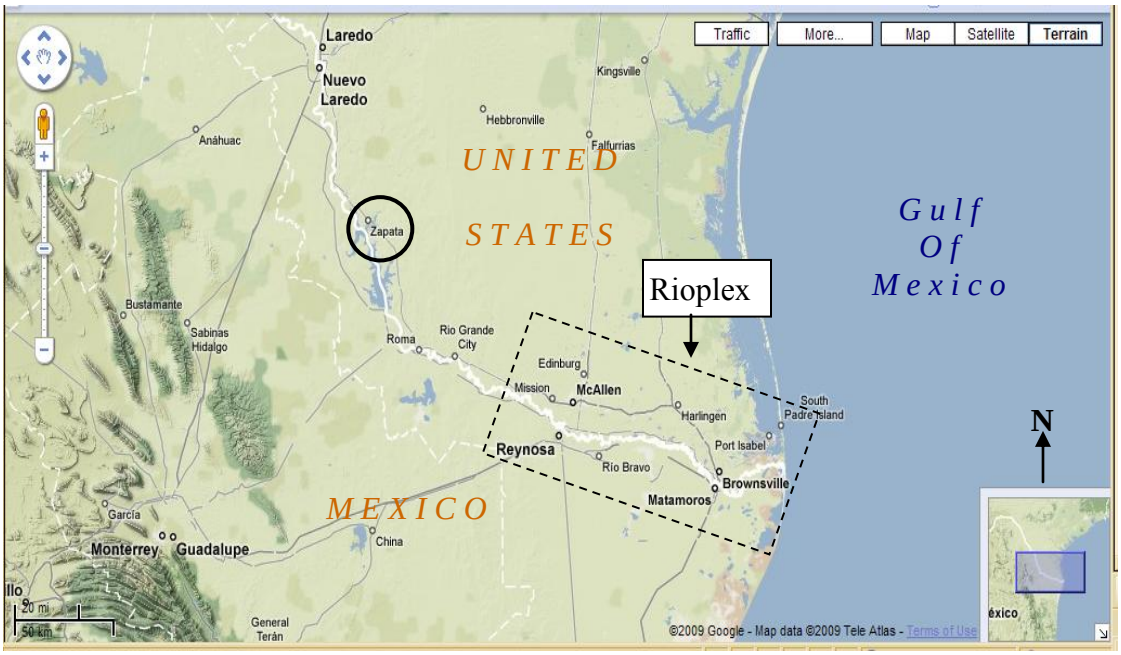

Figure 1. Map that illustrates Zapata, Texas (circle), the Rioplex area (dotted rectangular) and western Gulf of Mexico. *Source*: 2009 Google Earth – Map data and Tele Atlas

Besides the South Texas region, the area south of the Rio Grande referred to as northeast Mexico was also considered part of the study. The reasoning was the expectation that certain meteorological conditions would advect plumes from southern Mexico and Central America over northeast Mexico into the South Texas region and beyond.

Northeast Mexico covers three Mexican states, i.e., Coahuila, Nuevo León, and Tamaulipas (see figure 2). The 2005 Mexican census reports the populations of Coahuila to be 2.5 million, Nuevo León 4.2 million, and Tamaulipas 3 million (INEGI, 2005). Coahuila and Nuevo León are similar in vegetation, topography and climate. In contrast,

Tamaulipas, which is the Mexican state that where the south side of Rioplex, has coastal and subtropical conditions. The Sierra Madre Oriental mountain range crosses all three states and runs parallel to the gulf coast and acts as a boundary between the lowlands of Tamaulipas and the higher elevation of Nuevo León and the state of Coahuila. Coahuila and Nuevo León's have dry climate that limits agriculture activities to those that can provide irrigation. Consequently, many areas are dedicated to cattle ranching, including some portions of Tamaulipas. Deforesting is limited by the low number of forests and the difficulty to access them because of the mountain range. Tamaulipas is a more diverse state in both topography and vegetation. It has mountains, coastland, scrubs, tropical areas, and forests (Mendoza et al, 2003).

In the spring, northeast Mexico is primarily very dry between the months of January and April. In fact, Nuevo León receives less than 180 mm of rain and Tamaulipas even less. After five months of dry condition, it is until April when there is a drastic increase in temperature and makes the vegetation more prone for fire ignition. (Mendoza et al, 2003).

Of more importance, though is the seasonal biomass burning that occurs in southern Mexico and Central America during the same time of the year due to the significantly higher amount of biomass in this area which range from agricultural areas to mountainous and tropical forests. Figure 3, shows a map that approximately indicates these two regions, including northeastern Mexico and central Mexico, with a dashed-lined square and oval circles. The Central Mexico region near Mexico City which includes the state of Puebla, Veracruz, Jalisco and other residing states is a region that should not be disregarded as possible sources of biomass-burning, including urban and

power plant emissions. Emissions from such sources can be transported towards Rioplex and other areas of Texas. The Central Mexico is geographically located in the path of biomass-burning plumes from Southern Mexico and Central America. However, the Sierra Madre is a natural barrier for the plumes to overcome and the right meteorological conditions would have to exist for the plumes to be transported to the study area.

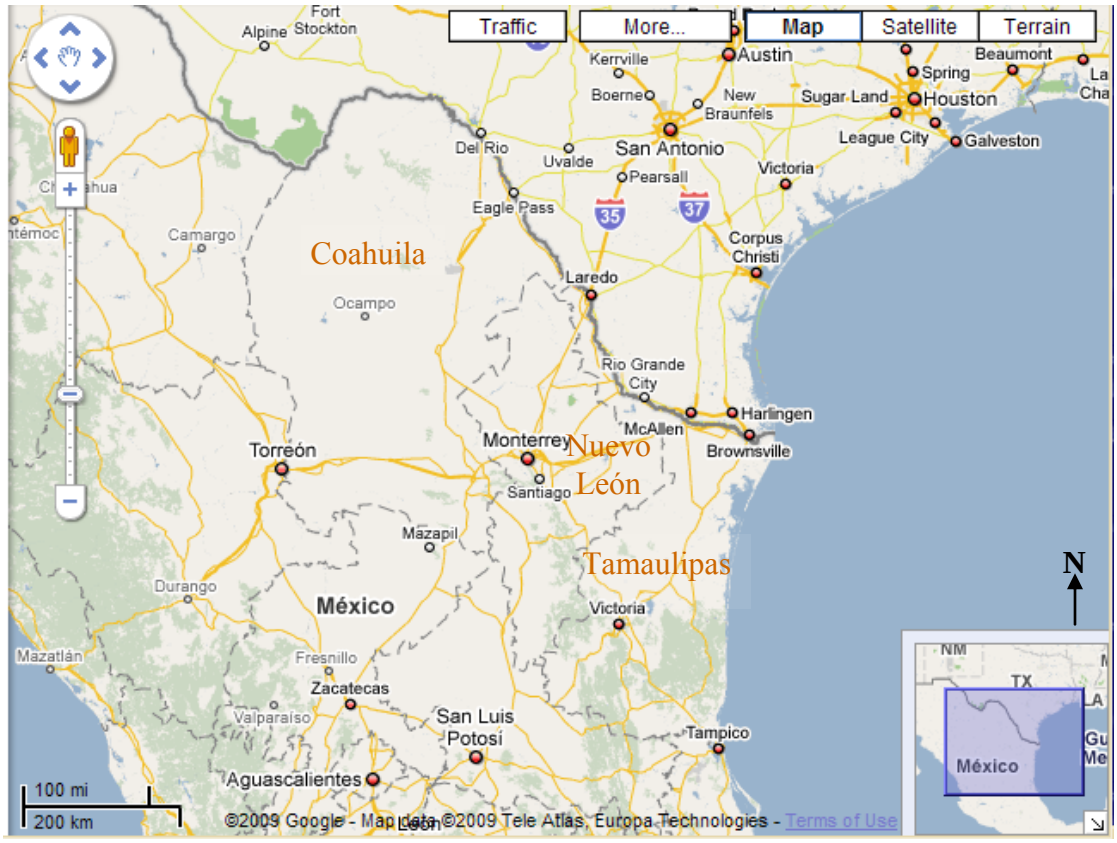

Figure 2. Map illustrating northeastern Mexico and part of Texas. *Source:* Generated with 2009 Google Earth – Map data , Tele Atlas, and Europa Technologies

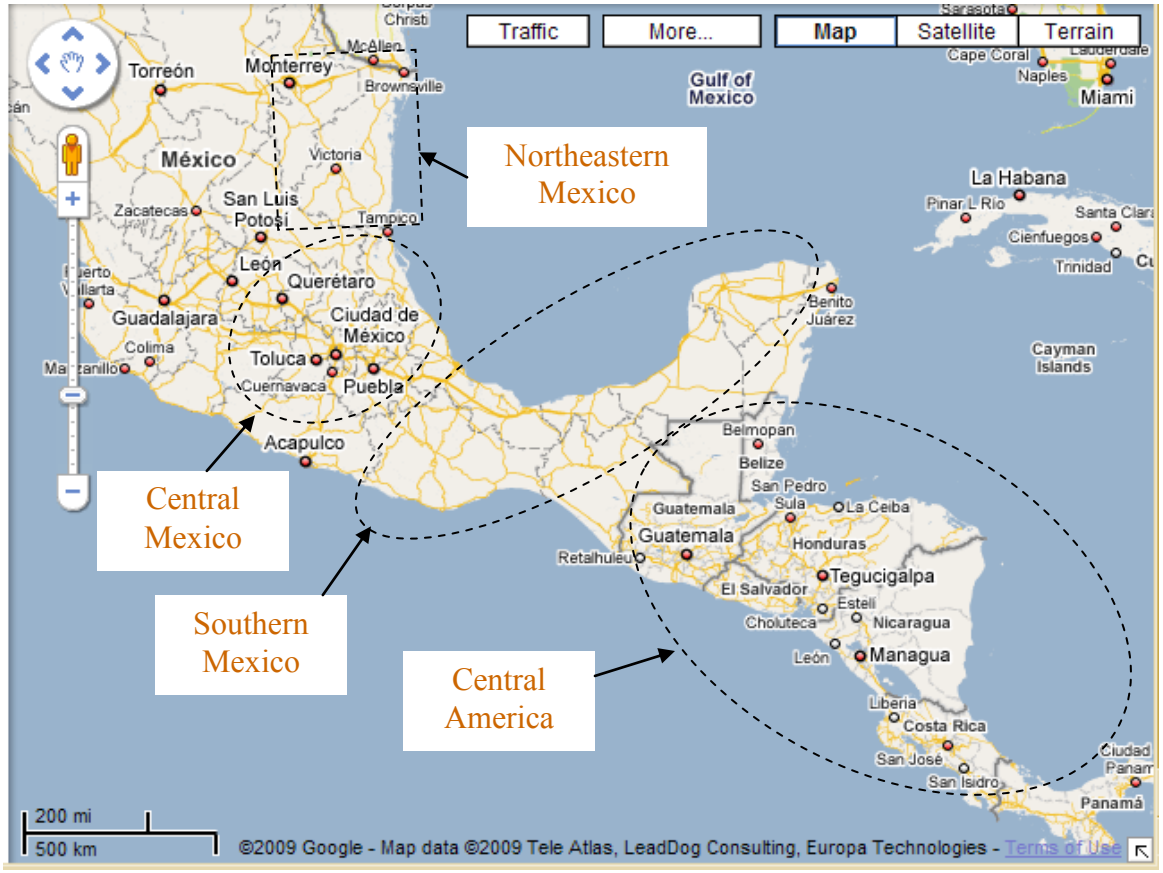

Figure 3. Map the depicts northeastern Mexico, southern Mexico and Central America. *Source:* Generated with 2009 Google – Map data, and Tele Atlas, LeadDog Consulting, and Europa Technologies

Measurement Platform

The measurement platform was a Piper Aztec multi-engine aircraft. The aircraft has an endurance of 7 hours with 30 minute reserve. Sampling speed is typically 62 m s^{-1} (120 knots). The payload maximum weight is 290 kg (640 lb) and has seating capacity for 1 pilot and 1 scientist. The aircraft also has two sine wave inverters capable of generating 2 kW of power. However they are not operated at 100% capacity, so the operating lives are not shortened. Figure 4 shows the aircraft in flight, sampling inlets and a side-view of the aircraft during a pre-flight calibration at the Zapata County airport.

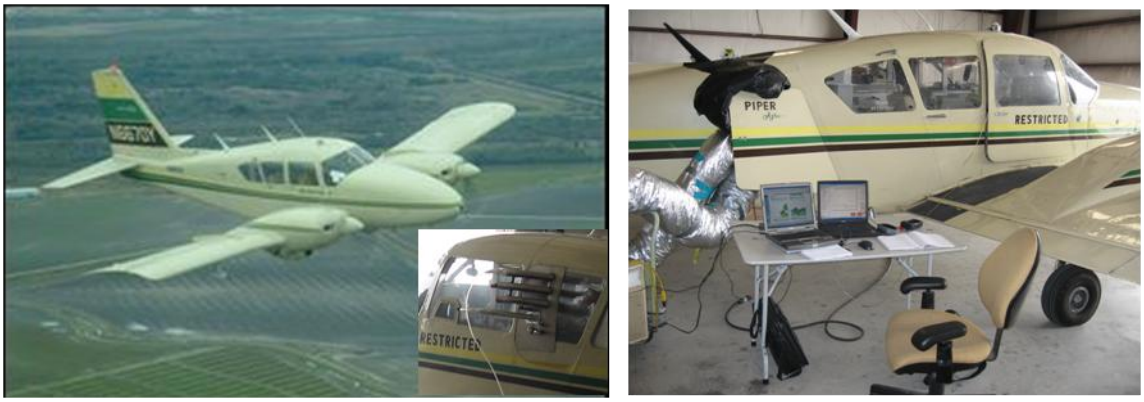

Figure 4. Left, Aircraft in flight and an inset of the sampling inlets; right, Side-view of aircraft

Measurements

The aircraft instrument payload consisted of a wide array of measurement. It included nitric oxide (NO), nitrogen dioxide (NO_2), reactive nitrogen (NO_y), carbon monoxide (CO), sulfur dioxide (SO_2), ozone (O_3), particle light scattering at three different wavelengths (700 nm, 550 nm, 450 nm), an aerosol spectrometer, filter samples (for inorganic aerosol composition species) and whole air samples (for volatile organic compounds [VOC]). In addition, aircraft position (latitude, longitude, and altitude) and meteorological measurements (wind direction and speed, air temperature, relative humidity, and atmospheric pressure) were made with an Aircraft-Integrated Meteorological Measurement System (AIMMS -20). A full description for each measurement is beyond the scope of this thesis and only CO, O_3, VOCs whole air samples and inorganic aerosol composition species (Na^+, NH_4^+, K^+, Ca^+, Mg^+, Cl^-, NO_3^- ,$(COO^-)_2$ and SO_4^{2-}) will be discussed.

Carbon Monoxide

Carbon monoxide (CO) mixing ratios were determined with a vacuum ultraviolet fluorescence measurement (VUV) technique. The instrument is based on the fluorescence of CO in ultraviolet range of 150 nm. The light wavelength range between 160 nm and 190 nm is detected by a VUV photomultiplier followed by a fast counter. The VUV light that excites the CO molecules is generated by a lamp that uses an Argon/CO_2 gas mixture. The instrument is commercially available (AL5001) and is manufactured by AeroLaser GmbH, Garmisch-Partenkirchen, Germany.

Because of the water effect on the instrument baseline, a matrix zero was performed on the CO instrument. This process consists of sampled air being diverted to a heated catalyst (palladium on alumina) that is temperature controlled at 500°C. In this converter, CO is converted to CO_2, but the ambient water vapor is passed quantitatively. This process occurred automatically every 10 minutes for 30 seconds. The interpolated zero level is subtracted from the signal in data processing. The instrument was calibrated with an undiluted Scott-Marrin 567 ppbgas standard that was traceable to NIST (National Institute of Standards and Technology) with an accuracy of ± 2%. The detection limit for this data set is estimated to be 21 ppbv and is based on the variability in the determination of the field zero air levels. The estimated accuracy for the measurement is 5%.

Ozone

Ozone (O_3) mixing ratios were determined with a 2B Technologies (Boulder, CO) dual-beam UV photometer wherein the absorption of 254 nm radiation by the continuously flowing sample gas is related to O_3 concentration by a known absorption coefficient. In the dual beam instrument, UV light intensity measurements I_o (O_3-

scrubbed air) and I (unscrubbed air) are made simultaneously, allowing for faster response (~2 seconds). The method is both pressure and temperature dependent and corrected for both using temperature and pressure mounted in the instrument.

The O_3 instrument was periodically compared with multi-point calibrations (concentrations between 25 and 250 ppb) against a TEI 49C-PS primary ozone standard. In turn, the 49C-PS's photometer was compared with the Region 6 EPA laboratory's NIST traceable photometer. The zero level of the instrument was assessed during the pre-flight calibrations. The value observed is entered into the data processing procedure and is subtracted from the observed value. The detection limit for this data set is estimated to be 1 ppbv and is based on the variability in the determination of the field zero air levels. The estimated accuracy for the measurement is 4%.

VOCs

During the flights air samples of VOC were collected in 1 L 2-valve electropolished stainless steel canisters (Fäth, Eschau-Hobbach, Germany). Analysis was performed by the University of Houston using a Perkin-Elmer VOC-system consisting of a Clarus 500 gas chromatograph with heart cut device and equipped with two flame ionization detectors and two columns (Alumina PLOT column and BP-1) for multi-dimensional gas chromatography. Samples were preconcentrated on a cold trap which contains carbonaceous sorbents and subsequently desorbed by a Turbomatrix 650 Thermal Desorber. Water was removed through a Nafion dryer. A detailed description of the system can be found in Leuchner and Rappengück (2009).

The VOC GC system was calibrated using a 30 component EU Directive ozone precursor mixture provided by the UK National Physical Laboratory (NPL). This

mixture contained VOC in mixing ratios of about 5 ppbv and has been found to be very stable over long time periods. Uncertainties are stated to be below 2% (95% confidence limit). The NPL standard was used to verify the stability of the linear carbon response of the GC. A deviation of ±5% from the average carbon response is acceptable with the exception of acetylene which has shown systematically larger deviations. For identification purposes a 72 VOC standard in the range of 0.2-11.3 ppbv (stated uncertainty below 5%) provided by the National Center for Atmospheric Research (NCAR) was used. This standard allowed optimum identification and has been successfully used in recent intercomparisons (Rappenglück et al., 2006). Both standards do not need any dilution and thus minimize errors and uncertainties arising from dilution methods. Instrument response is correlated with concentration for each hydrocarbon species in the standard based on peak areas. The GC system is able to process up to 8 canisters in a sequence. In each sequence one canister contains the NPL mixture and another one the NCAR mixture. Calibration is performed for each sequence.

The combined standard uncertainty for alkanes is 7.3%, for alkenes 14.3%, alkynes 7.3%, and for aromatics 14.4%. For mixing rations below 0.1 ppb, the combined uncertainty is 70% regardless of the VOC group.

Filters

The filters samples were analyzed at the University of New Hampshire (UNH) ion chromatograph laboratory. The UNH Ion Chromatography (IC) systems were calibrated with NIST traceable liquid standards. These standards contain sodium (Na^+), ammonium (NH_4^+), potassium (K^+), calcium (Ca^+), magnesium (Mg^+), chloride (Cl^-), nitrate (NO_3^-), sulfate (SO_4^{2-}), oxalate $(COO^-)_2$, formate ($CHOO^-$)and acetate ($[CH_3COO]^-$) in mixing

ratios of about 5 ppbv and have been found to be very stable over long time periods. These standards were diluted to provide a 10 point calibration curve of the range of the analytical concentrations. Uncertainties are stated to be below 2% (95% confidence limit). The aerosol samples were collected on a 90-mM teflon membrane with 1 μm nominal pore size in a custom made open-face teflon filter holder with a polypropylene backup filter support that results in 70 mb pressure drop. Aerosol samples were stored in a freezer for less than a week until the water-soluble fraction was extracted in teflon tubes by application of 200 μL of MeOH and then two 5.0 mL aliquots of deionized water. Aerosol extracts were preserved with 100 μl of $CHCl_3$ and stored at 5ºC in 30-mL high-density polyethylene amber bottles.

The limits of detection limit for the filter analyzed species are Na^+ 60 pptv, NH_4^+ 60 pptv, K^+ 30 pptv, Ca^+ 60 pptv, Mg^+ 60 pptv, Cl^- 60 pptv, NO_3^-12 pptv, $(COO^-)_2$ 8 pptv, and SO_4^{2-} 30 pptv. They are based on using three times the average standard deviation for a 30 minute collection period and a sampling rate of 100 standard liters per minute. The accuracies for each species are Na^+ 60%, NH_4^+ 8%, K^+ 33%, Ca^+ 40%, Mg^+ 40%, Cl^- 60%, NO_3^-6%, $(COO^-)_2$ 18%, and SO_4^{2-} 5%.

Meteorological Measurements

The meteorological measurements of wind speed (WS), wind direction (WD), temperature (T), pressure (P), and relative humidity (RH) were measured with an AIMMS-20 manufactured by Aventech Research in Ontario, Canada. The winds were measured by relating aircraft motion, determined by GPS-derived position, to pressure changes measured in the three axes on the probe mounted under the right wing of the aircraft. Within the probe, ambient temperature was measured using an onboard platinum

resistance thermometer and relative humidity was measured using a solid-state sensor. The wind data were collected by the AIMMS-20 data acquisition system at 16 Hz and were subsequently reported at 5 second.

Flight Plans

In this subsection, two types of flight of plans are discussed, flight plan A which was primarily to collect baseline data without the influence of biomass-burning plumes and flight plan B which was to collect data with the influence of biomass-burning plumes.

Flight Plan A

This type of flight plan was designed to establish a baseline that would represent a transported air mass from Mexico and/or the Gulf of Mexico with no influence from long range smoke plumes from Mexico and/or Central America. It focuses on taking samples at different altitudes over land, approximately parallel to the Rio Grande River and to the north of it. The objective was to collect data over land within the CBL (Convective Boundary Layer) and at multiple altitudes downwind of urban and point sources along the US-Mexican border.

The required forecast meteorological conditions before a science flight was launched were for the wind direction to be between 135° and 225°, wind speeds between 5 and 15 knots (2.6 and 7.7 m s^{-1})and the sky coverage clear below 15000 ft (457 m). Figure 5 illustrates a map of the South Texas region and the aircraft's proposed flight path that primarily runs along the US-Mexico border (i.e., Rio Grande River). The bold

magenta line depicts the proposed flight path of the aircraft from Nuevo Laredo to the western Gulf of Mexico within the CBL (Convective Boundary Layer). In addition, the following is a list that sequentially describes the path of aircraft in the flight plan:

1. Depart from Zapata County Airport (T86) to arrive at the initial flight track entry point located 0.8 km (0.5 mile) east of the Rio Grande River, 1.6 km (5 mi) north of Laredo International airport (KLRD).
2. On the southern flight track, the aircraft will sample at 457 m (1500 ft) MSL within the CBL.
3. The southbound flight track will be flown from the flight track entry point, parallel to the Rio Grande River, to a procedure turn approximately 40 km (25 mi) east of Brownsville/South Padre Island International Airport (KBRO).
4. The procedure turn will establish the aircraft on a reciprocal ground track while climbing to an altitude of 1524 m (5000 ft) MSL or at an altitude above the CBL.
5. The northern flight track will be a reversal of the southern flight track alongside the Rio Grande River.
6. The sampling track will end 5 mi north of Laredo International Airport (KLRD).
7. The flight will terminate at Zapata County Airport (T86).

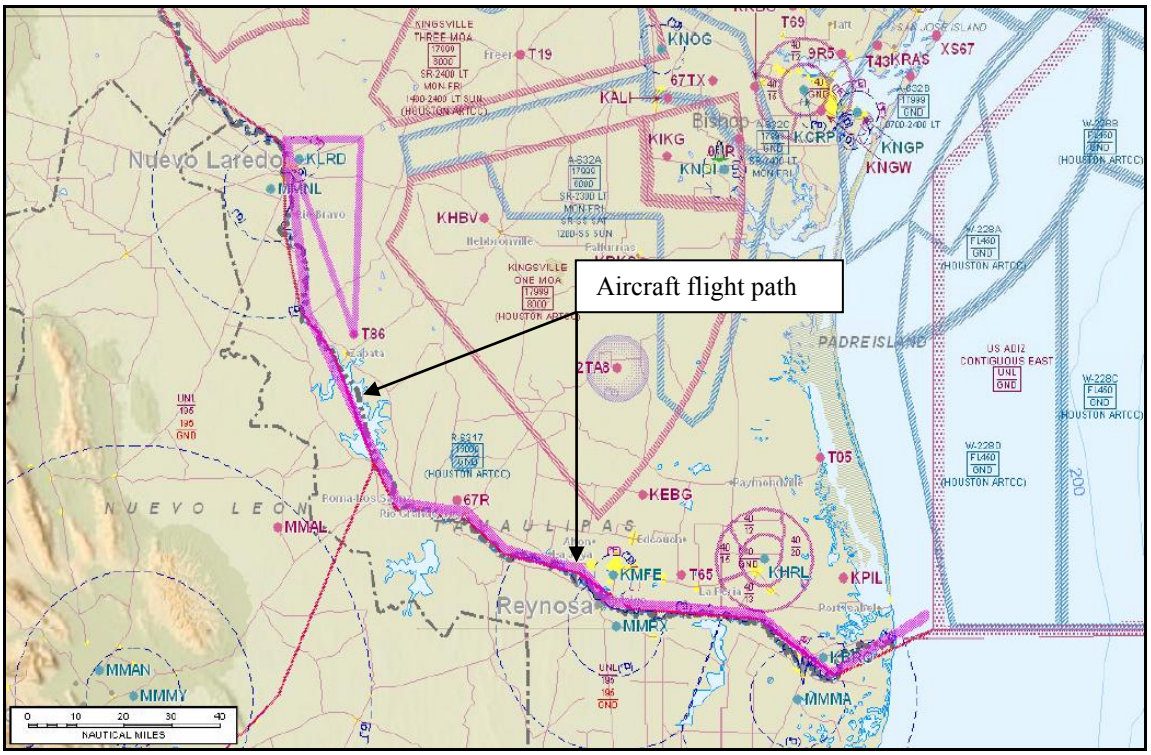

Figure 5. Map of South Texas region illustrating Flight plan A. *Source*: Generated with Jeppesen's, Flite Star® software

Flight Plan B

This type of flight plan was designed to collect data from smoke plumes from biomass origin either from Mexico and/or Central America that that were advected over the South Texas region and adjacent area of the western Gulf of Mexico. In addition, it can also be used as a flight plan to establish a baseline of the measured pollutants from cities and point sources sited along the Rio Grande River. The flight plan focuses on sampling within the CBL and above the CBL, and over land. The objective was to collect data at multiple altitudes over land downwind of urban and point sources located along the US-Mexico border.

The required forecast meteorological conditions before a science flight was launched for the wind direction to be between 135° and 225°, wind speeds between 2.6 and 7.7 m (5 and 15 knots) and the sky coverage clear below 4572 m (15000 ft). Figure 6 illustrates a map of the South Texas region and the aircraft's proposed flight path that is offset to the north of the US-Mexico border (i.e., Rio Grande River). It also includes a flight path segment over the western Gulf of Mexico. Extending the flight path to the western Gulf of Mexico increases the geographical area to sample smoke plumes from biomass burning origin. "Step-ladder" passes over the same flight path over the Gulf of Mexico provides vertical profile data and the identification of entrained smoke layers. The bold magenta line indicates the proposed flight path of the aircraft from the Zapata County airport (T86) to the western Gulf of Mexico. In addition, the following is a list that sequentially describes the path of aircraft in the flight plan:

1. Depart from Zapata County Airport (T-86) to arrive at the initial flight track entry point located 20.7 mi (18 nm) east of Brownsville / South Padre Island International Airport (KBRO).
2. The first sampling leg of the flight will begin overhead the entry-point at 152 m (500 ft) MSL and will continue at that altitude to a location 57.5 mi (50 nm) east.
3. A 180 degree procedure turn will establish the aircraft on the second sampling leg of the flight plan at an altitude of 1524 m (5000 ft) MSL westbound. Sampling will be conducted at this altitude to a position overhead the sampling leg entry point.
4. The third sampling leg of the flight will begin overhead the entry point at 1000 m (10000 ft) MSL and will continue at that altitude to a location 57.5 mi (50 nm) east.
5. A 180 degree procedure turn will establish the aircraft on the fourth sampling leg of the flight plan at an altitude of 4572 m (15000 ft) MSL westbound. Sampling will be conducted at this altitude to a position overhead the entry point.
6. Concluding the fourth leg, the aircraft will return to Zapata County Airport (T86).

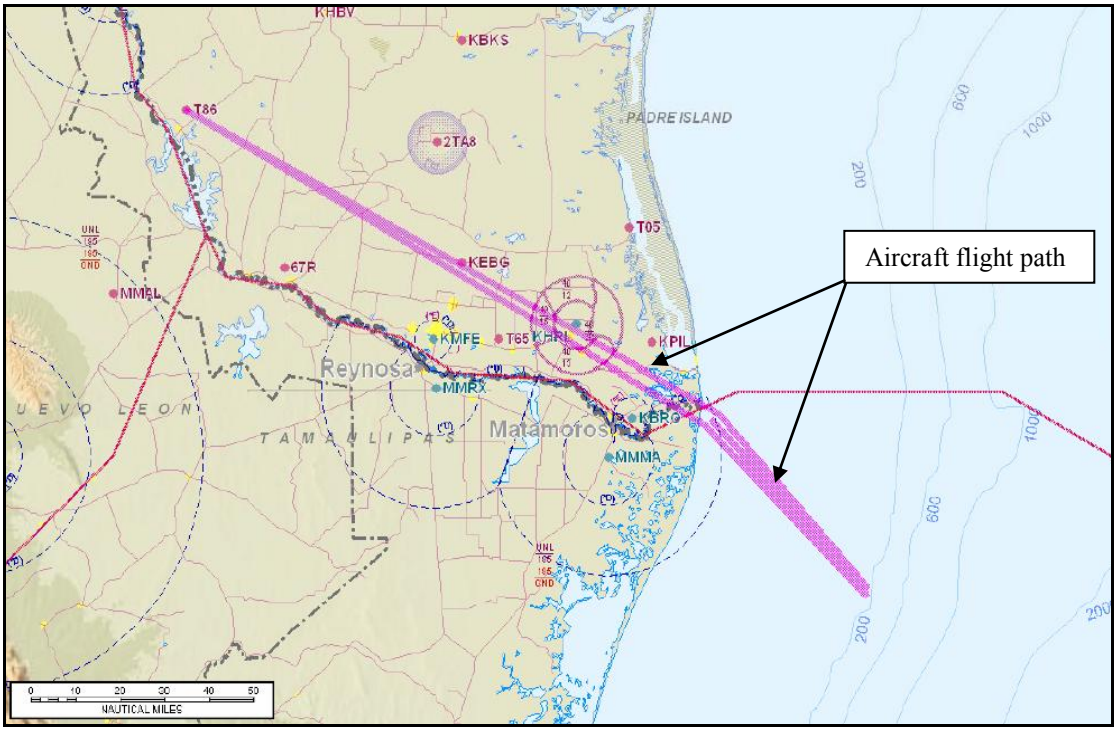

Figure 6. Map of South Texas region US-Mexico border. *Source*: Generated with Jeppesen's, Flite Star® software

CHAPTER THREE

Results and Discussion

Flight A – April 23, 2007

This science flight was the first of 5 flights that were flown during the first smoke episode, part of a broader study. The expectation was that smoke would begin drifting over the Rio Grande Valley from the Gulf of Mexico and the rest of the south Texas region. The flight was initiated due to 48-hour backward trajectories based on NOAA's HYSPLIT model (Draxler and Rolph, 2003) National Weather Service forcansts indicating synoptic wind flow from the Gulf of Mexico and the Yucatan peninsula (figure 7). In fact, the lower altitude trajectories between 100 m, 500 m and 1000 m traced the air mass to the Yucatan. Whereas, the higher altitude trajectories between 1500 m and 2500 m showed the air mass had been advected over northeast Mexico. Equally important, were the increase in the number of fires, or hot spots, detected by the GOES and MODIS satellites in the Yucatan and Central America (see figure 8). The NAAPS (Navy Aerosol Analysis and Prediction System) global aerosol model also showed a smoke plume over southern Mexico (see figure 8), and the daily NOAA/NESDIS (National Environmental Satellite, Data, and Information Service) text narrative briefing reported dispersed smoke that covered much of the western Gulf of Mexico (NOAA, 2006). All sources of information available indicated smoke drifting towards the South Texas, northeastern Mexico, and the Western Gulf of Mexico regions. However due to cloud coverage, satellites (i.e., visible) had difficulty detecting the smoke, especially over land.

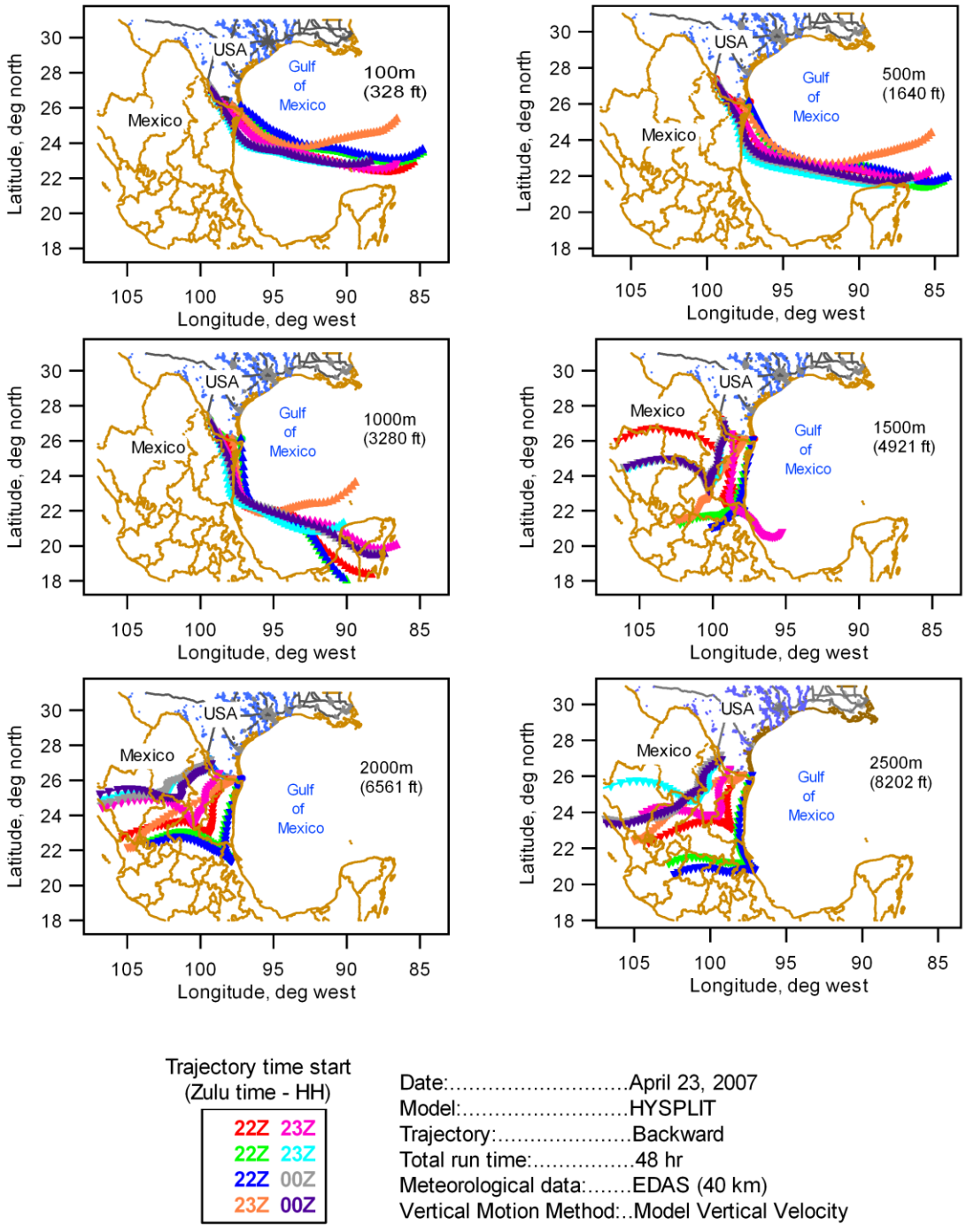

Figure 7. Six maps of 48-hr backward trajectories that began at the altitudes of 100 m, 500 m, 1000 m, 1500 m, 2000 m, and 2500 m. Zulu time is the same as Greenwich Mean Time (GMT). The trajectories originate from aircraft flight path over different geographic locations along the US-Mexico border. *Source:* Adapted data from NOAA HYSPLIT model

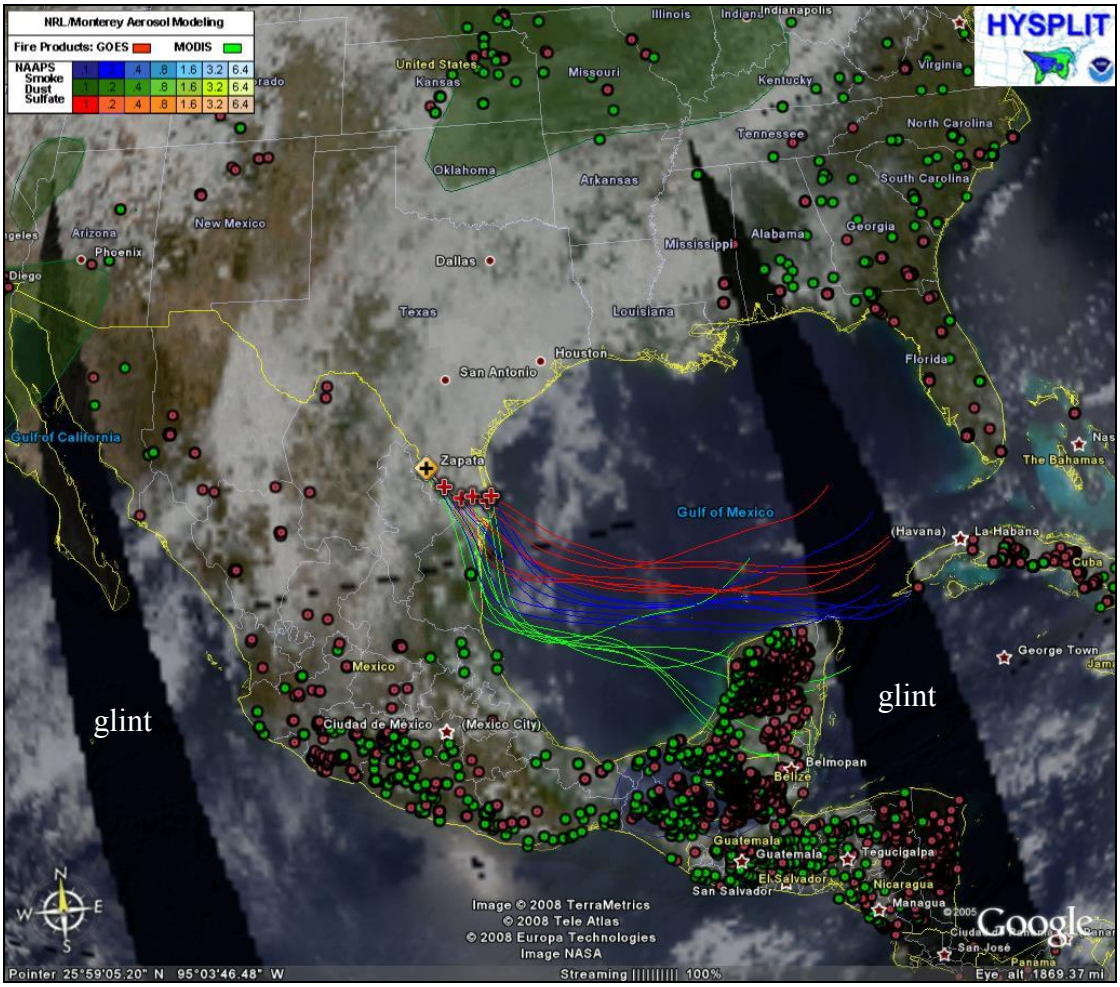

Figure 8. Map illustrating HYSPLIT (48-hr) backward trajectories (red, blue and green lines), fire detections by GOES (red dot symbols) and MODIS (green dot symbols) satellites, and NAAPS aerosol modeling of smoke, dust and sulfate, over a MODIS satellite image. The backward trajectories originate (red-cross symbols) from the aircraft flight path in the south Texas region (red cross symbols). The red lines represent trajectories that began at 100 m (328 ft), blue lines at 500 m (1640 ft), and green lines at 1000 m (3280 ft). The NAAPS model shows smoke in southern Mexico by the transparent slate blue color. *Source:* Image generated by 2008 TerraMetrics, Tele Atlas, Europa Technologies, Google Earth, and NASA.

The aircraft departed the Zapata County airport in the late afternoon and flew within the CBL at approximately 305 m (1000 ft) MSL (Mean Sea Level) parallel to the Rio Grande River, i.e. U.S.-Mexico border, to the Gulf of Mexico. As illustrated in figure 9 the wind direction is from the southeast at 305 m (1000 ft) MSL and from the south-southwest at 2090 m (6860 ft).

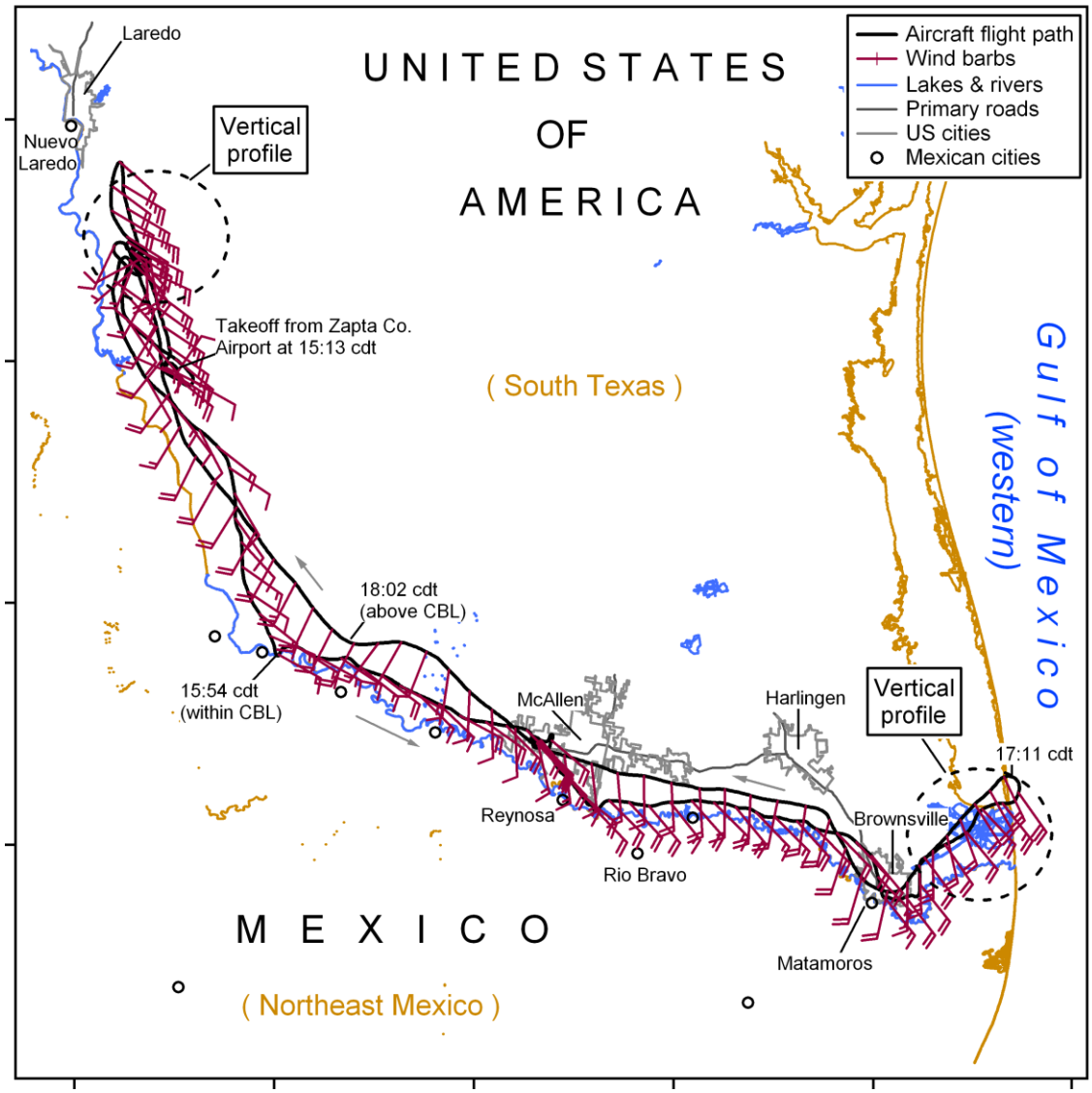

Figure 9. Map of aircraft path (black trace) and wind barbs. The black dashed circles are the approximate geographic locations where the vertical profiles were conducted.

The sky conditions were mostly cloudy to overcast (see figure 8). Upon reaching the coast, the aircraft reversed its course and began an en route ascent to approximately 2073 m (6800 ft) MSL. Scattered clouds were observed below 305 m (1000 ft) with increasing intensity towards the Gulf of Mexico and an overcast layer at approximately 1981 m (6500 ft) MSL.

The vertical profiles were flown to characterize the vertical structure of the atmosphere and most importantly to find entrained smoke layers. One vertical profile was flown over the Texas coast adjacent to Port Isabel and the other adjacent to the Zapata County airport (see figure 9). The profile near the coast revealed elevated mixing ratios of CO, including increased light scattering (B_{sp}) by particles in a layer between 1900 ft (579 m) MSL and 6000 ft (1829 m) MSL (see figure 10). Maximum enhancements were observed in a layer between 1900-4000 ft (579 – 1219 m). According to the backward air trajectories in figure 7 and figure 8, air masses found in this layer most likely passed Yucatan and Campeche. At 6700 ft (2042 m) MSL, most trace gases and relative humidity decreased substantially (figure 10 and figure 12), which is an indication of the height of the CBL. O_3 did not decrease. In fact, it increases slightly compared to the lower altitudes. This can be attributed to strongly absorbing aerosols in the smoke that can reduce actinic flux at the surface while strongly scattering aerosols can lead to an increase in actinic flux *(*Dickerson et al., 1997; Jacobson, 1998) or a lack of O_3 precursors (i.e., NO_x and VOCs).

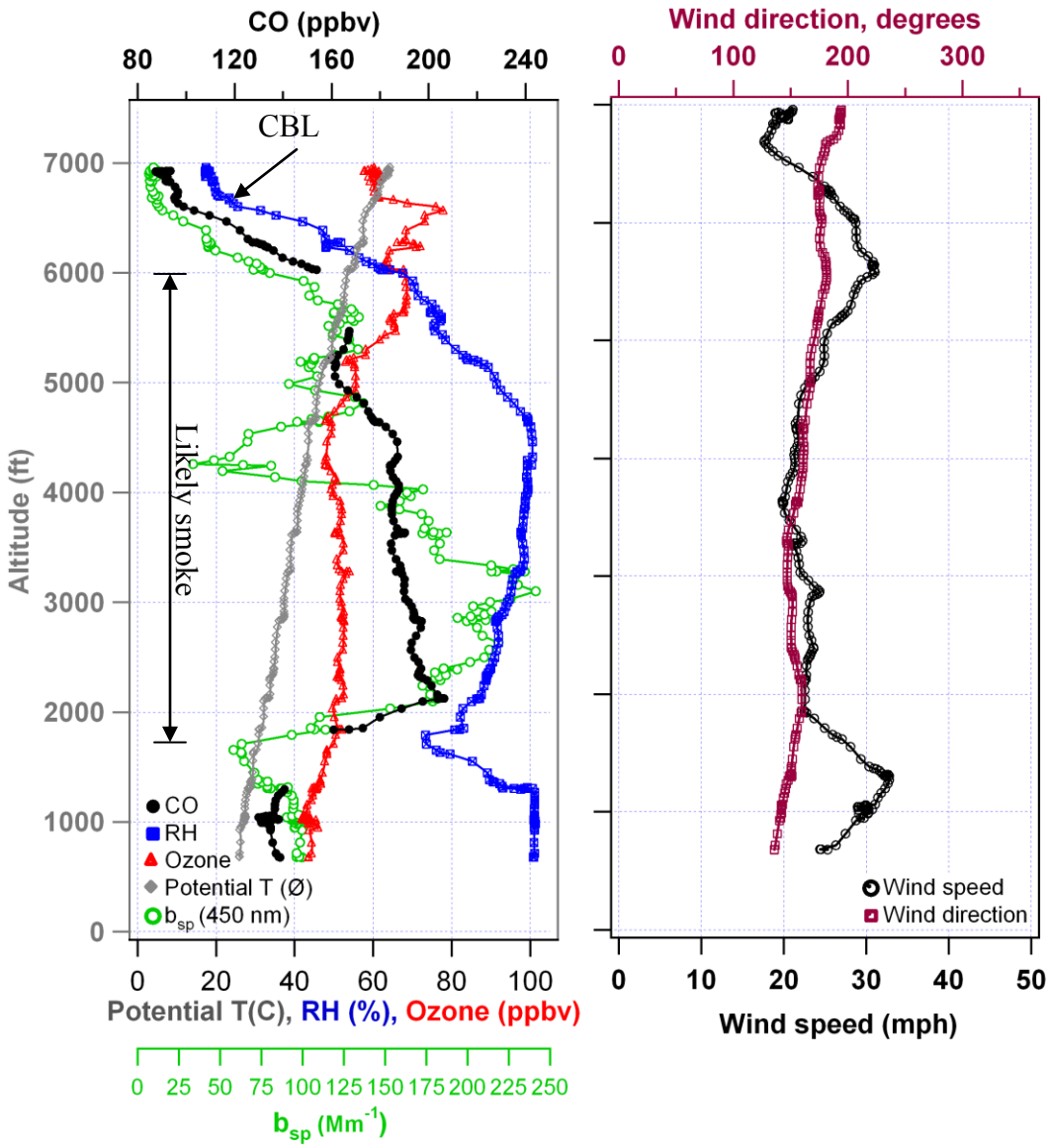

Figure 10. Vertical profile of trace gases and meteorological parameters over Texas coast at 1711 CDT on April 23, 2007

Thirty miles (48 km) northwest of McAllen, the aircraft made an ascent to 2743 m (9000 ft) MSL. Northwest of the Zapata County airport, the second vertical profile, a box-pattern descent, was performed to 244 m (800 ft) MSL. The CBL over that geographical area was at (1981 m) 6500 ft MSL (figure 11).

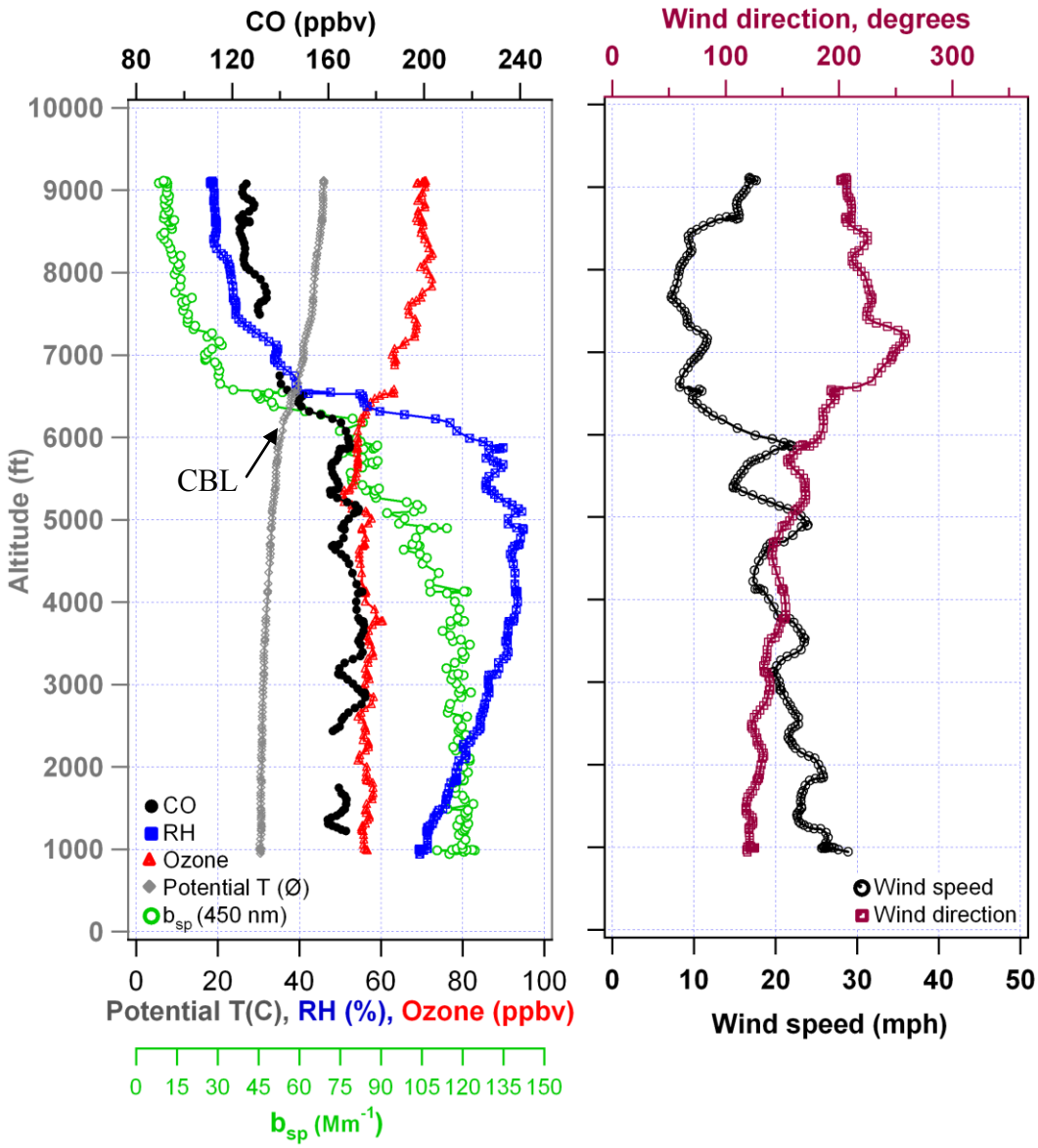

Figure 11. Vertical profile trace gases and meteorological parameters over Zapata County airport area at 18:28 CDT on April 23, 2007

The spatial plot of the flight path on figure 12 shows the highest mixing ratios (i.e., 213 ppbv) of CO near the coast during the flight. Above the CBL, mixing ratios of O_3 were significantly higher than within the CBL (figure 11), which can be an indication

of the presence of a different air mass. In fact, the HYSPLIT trajectories support this assumption.

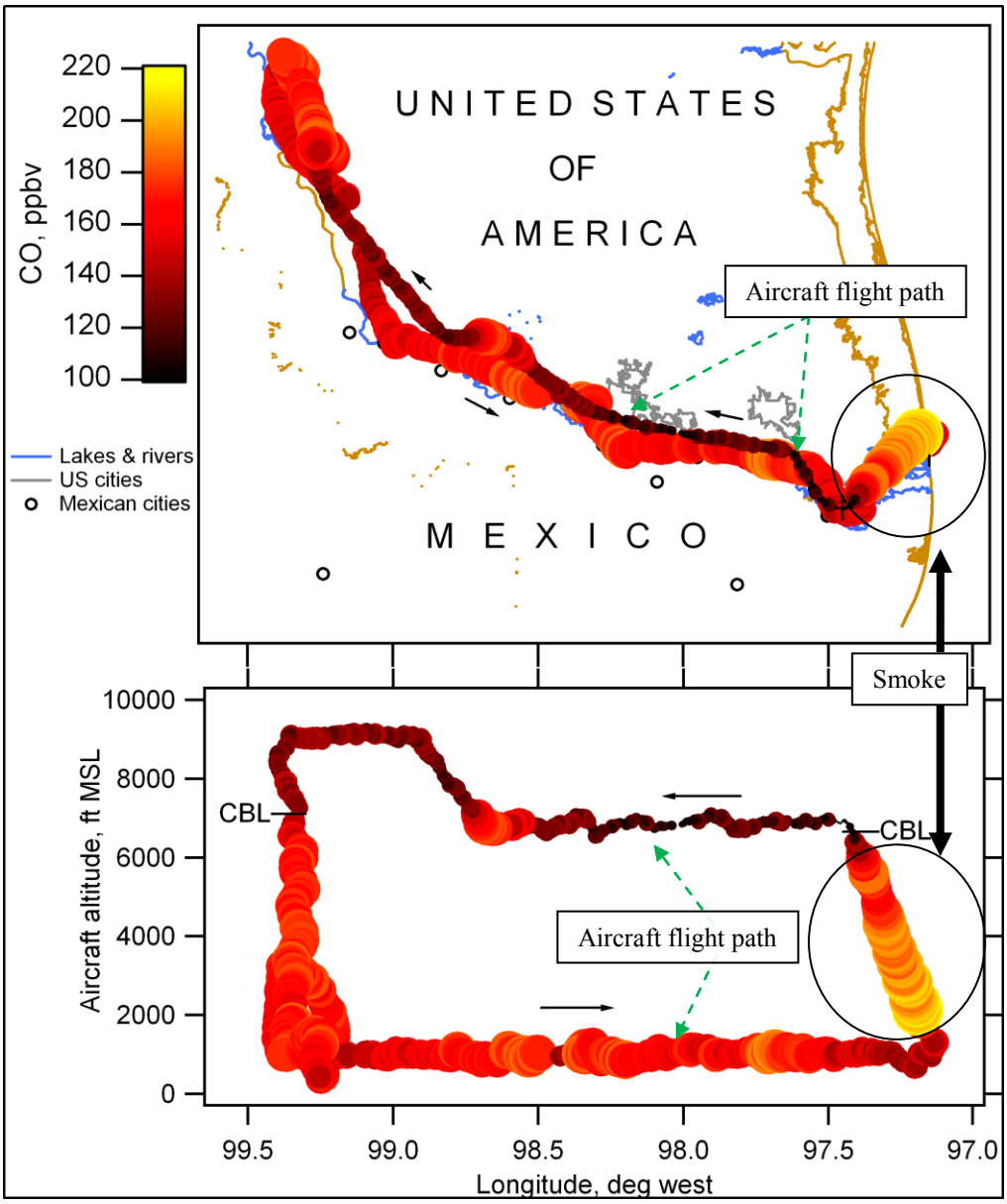

Figure 12. Aircraft flight path on April 23, 2007, color and symbol size color-coded by CO mixing ratio. The symbol size is proportional to CO mixing ratio.

Two aerosol filter samples (see table 2 and figure 13) were collected near the US-Mexico border flight paths, one from the Zapata, Texas area to the coast in the CBL and

the other above the CBL on the return flight. Both of these aerosol samples were quite clean, suggesting that the discrete filter sampling "missed" any brief encounters with plumes. The first (low altitude) sample did contain higher sea salt tracers (Na^+ and Cl^-), which is consistent with sampling from the marine boundary layer during the end of this filter exposure. Interestingly, the second sample collected at higher altitude on the way to Zapata was slightly higher in all species except the marine tracers. These two filters could be considered good continental and marine"background" samples (Alvarez et al., 2008).

Two VOC canisters sampled on this flight were near the city of McAllen, one within the CBL and the other above it. The map on figure 13 indicates where the VOC canisters were collected and includes a table of the filter samples collected. The results of the VOC canister samples are presented in table 1.

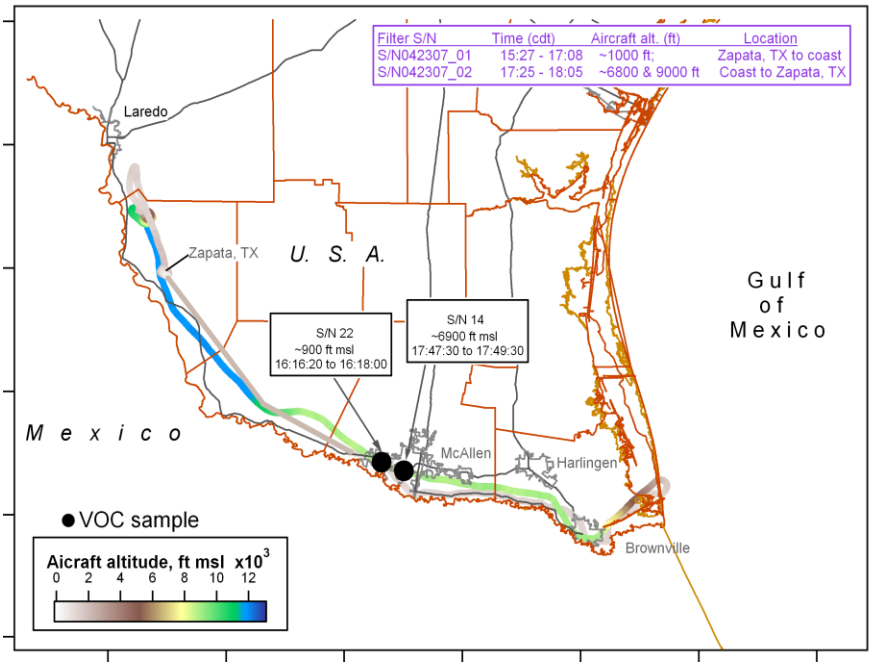

Figure 13. Map of aircraft flight path parallel to US-Mexico border with color-coded aircraft altitude along flight path. VOC canister samples are indicated with black dot symbols on the flight path. The table in the upper right corner lists filters that were sampled during the flight.

The contents of canister #22 reflected ambient conditions at about 900 ft (274 m) MSL within the CBL. The results indicate a total C_2-C_9 hydrocarbon mass of about 59 ppbC. C_3-C_4 alkanes, C_2-C_3 alkenes, as well as acetylene and toluene showed relatively enhanced values. This is an indication of local combustion processes. Canister #14 only contained 24 ppbC C_2-C_9 hydrocarbons. Ambient levels of most of the previously mentioned individual hydrocarbons decreased by a factor of 4-7 when compared to canister #22, which was sampled closer to the surface. Ratios of NMHC classes [based on ppbC] vs. the longer-lived CO [based on ppbv] in the two canister samples showed that both the alkene/CO and acetylene/CO ratios dropped by 2.8 and 2.9, respectively, from canister #22 to canister #14. The alkane/CO and aromatic/CO ratios dropped by 1.8 and 1.6, respectively. The isoprene/CO ratio increased slightly, by 10%. Also, the NMHC/NOx ratio [based on ppbC/ppbv] increased by almost 60%. Alkenes and acetylene have significantly different atmospheric lifetimes, but their corresponding ratios to CO showed the same decrease. This is a strong indication that the air masses sampled within the CBL and above the CBL had different origins. Further evidence of the dual sources of the air at these levels is that the isoprene/CO ratio increased slightly, possibly due to the shift from marine to continental source areas with increasing altitude, as indicated by the backward trajectories shown in figure 8. Unfortunately, no canister could be collected between 1900 – 4000 ft (579 m – 1219 m) MSL, where there was some evidence of a smoke layer, as shown in Figure 10 and Figure 12 (Alvarez et al., 2008).

Table 1. VOC Canister Analyses (VOC data courtesy of University of Houston)

mixing ratios [pptv]	Can S/N 22	Can S/N 14
ethane	1525	737
ethylene	847	165
propane	522	b.d.l.
propylene	282	85
i-butane	95	14
n-butane	244	49
acetylene	488	123
t-2-butene	11	b.d.l.
1-butene	35	13
i-butene	77	b.d.l.
c-2-butene	22	b.d.l.
cyc-pentane	16	12
i-pentane	367	110
n-pentane	63	b.d.l.
1,3-butadiene	b.d.l.	b.d.l.
cyc-pentene+2-me-2-butene	b.d.l.	b.d.l.
t-2-pentene	b.d.l.	b.d.l.
2-me-1-butene	13	b.d.l.
1-pentene	b.d.l.	b.d.l.
3-me-1-butene	b.d.l.	b.d.l.
c-2-pentene	b.d.l.	b.d.l.
2,2-dime-butane	10	b.d.l.
2,3-dime-butane	98	40
2-me-pentane	66	18
3-me-pentane	43	b.d.l.
isoprene	61	48
n-hexane	27	b.d.l.
c-3-hexene	b.d.l.	b.d.l.
t-2-hexene	b.d.l.	b.d.l.
c-2-hexene	b.d.l.	b.d.l.
me-cyc-pentane	b.d.l.	b.d.l.
2,4-dime-pentane	236	96
benzene	131	b.d.l.
cyc-hexane	16	12
2-me-hexane	b.d.l.	b.d.l.
2,3-dime-pentane	613	235
3-me-hexane	15	b.d.l.
2,2,4-trime-pentane+1-heptene	1729	756
n-heptane	5	17
2,3-dime-2-pentene	24	15
me-cyc-hexane	7	b.d.l.
2,3,4-trime-pentane	1092	558
toluene	1961	973
2-me-heptane	14	b.d.l.
4-me-heptane	b.d.l.	b.d.l.
3-me-heptane	7	b.d.l.
n-octane	6	b.d.l.
et-benzene	8	b.d.l.
m,p-xylene	63	b.d.l.
styrene	6	13
o-xylene	15	10
n-nonane	6	b.d.l.
i-prop-benzene	b.d.l.	b.d.l.
n-prop-benzene	7	b.d.l.
m-et-toluene	b.d.l.	b.d.l.
1,3,5-trime-benzene	b.d.l.	b.d.l.
o-et-toluene	19	6

Table 2: Aerosol Filter Analysis for 23 April 2007 Flight (Aerosol filter data courtesy University of New Hampshire).

Sample ID	042307_01	042307_02
Altitude (ft)	1011	6932
start-time (CDT)	15:27	17:25
stop-time (CDT)	17:08	18:05
Total volume sampled (L)	10090	4000
Na^+ (pptv)	426	175
NH_4^+ (pptv)	74	606
K^+ (pptv)	53	46
Mg^{2+} (pptv)	10	27
Ca^{2+} (pptv)	78	191
Cl^- (pptv)	307	150
NO_3^- (pptv)	18	61
SO_4^{2-} (pptv)	23	259
$C_2O_4^{-2}$ (pptv)	2	9
O_3 (ppbv)	47	64
NO (ppbv)	0.0	0.0
NO_2 (ppbv)	1.3	0.4
NOy (ppbv)	1.6	1.5
CO (ppbv)	154	117
SO_2 (ppbv)	0.1	0.1
Aerosol Backscatter @ 400 nm (Mm-1)	116	21
Air Temp (deg C)	27	21
RH (%)	78	27
WD (deg)	135	187
WS (mph)	19	18

Flight B – May 4, 2007

Low-level 48-hour backward trajectories (figure 14) indicating synoptic wind flow from the Gulf of Mexico and the Yucatan peninsula provided evidence of appropriate conditions for this science flight. There were also increased fires, or hot spots, detected by the GOES and MODIS satellites (figure 15). In addition, the NAAPS global aerosol model indicated a smoke plume drifting north from the Yucatan Peninsula

over the Gulf of Mexico (figure 15) and NOAA/NESDIS text narrative reported light to moderate residual smoke moving north across the western Gulf of Mexico into Texas and Louisiana (NOAA, 2006).

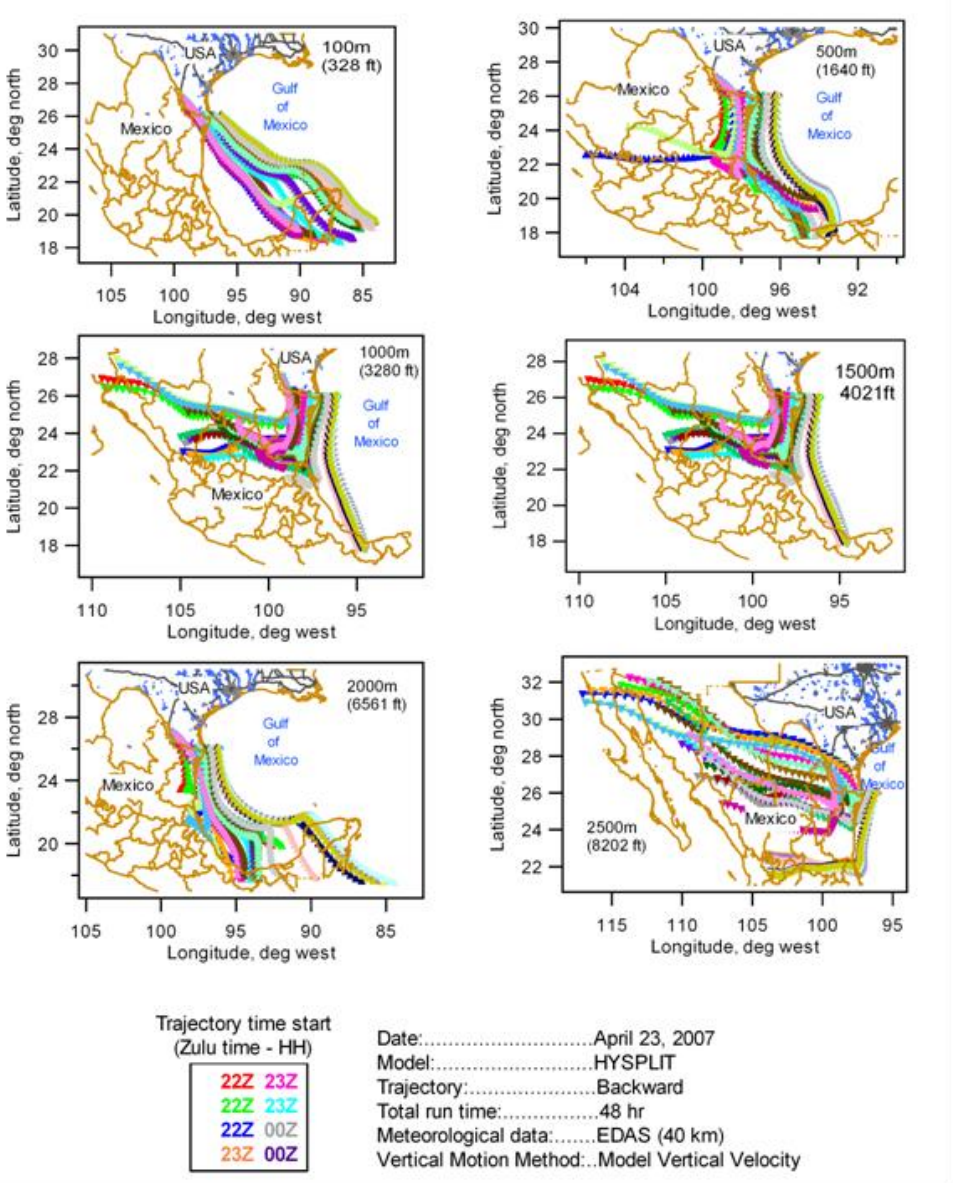

Figure 14. Six maps of 48-hour backward trajectories that began at the altitudes of 100 m (328 ft), 500 m (1640 ft), 994 m (3260 ft), 1500 m (4921 ft), 2000 m (6561 ft), and 2500 m (8202 ft) are presented. Zulu time is the same as Greenwich Mean Time (GMT). The trajectories originate at different geographic locations where the aircraft was flying. The time that the trajectory was begun is indicated in the color-coded legend. *Source:* Adapted data from NOAA HYSPLIT model

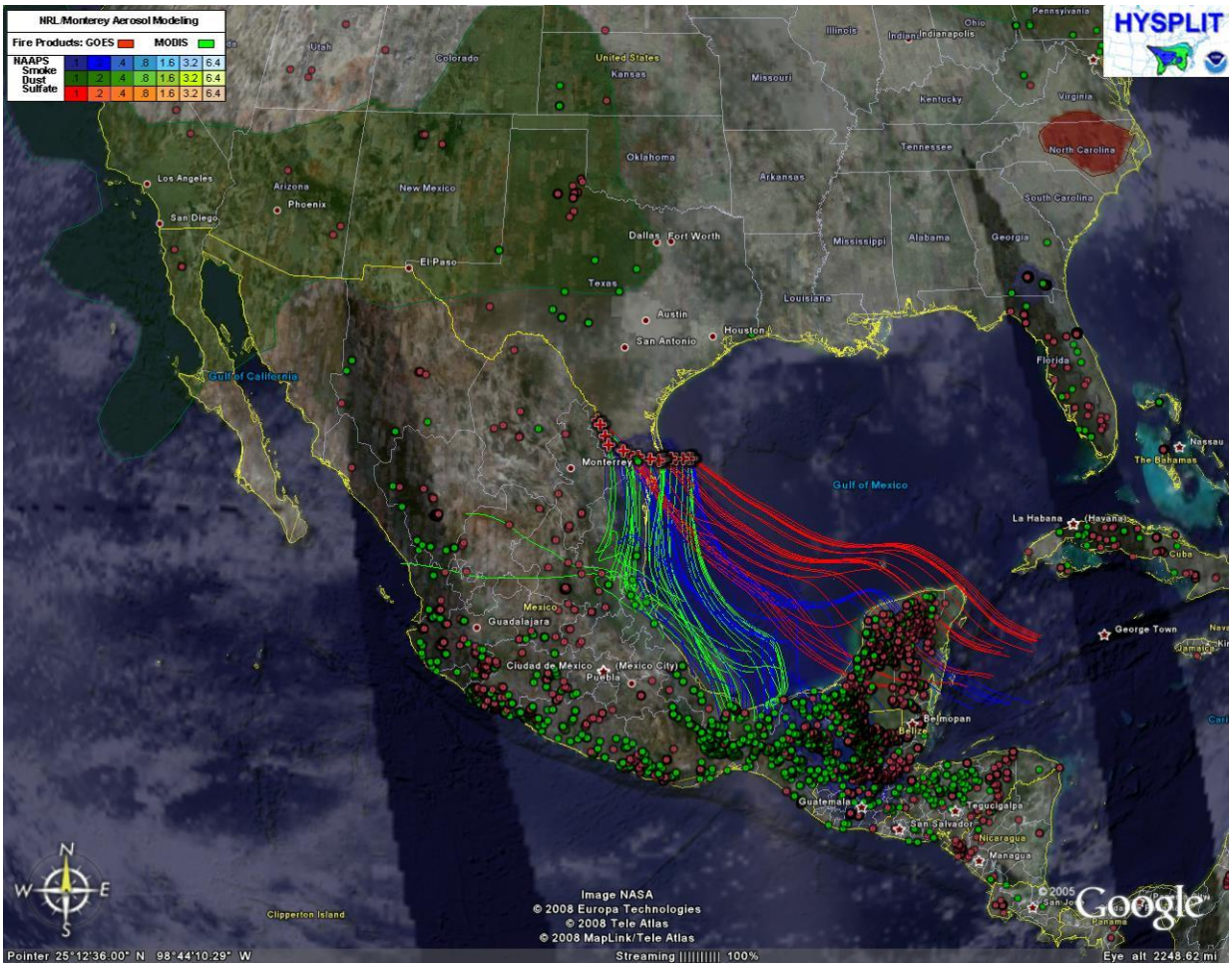

Figure 15. Google® map illustrating Hysplit (48-hr) backward trajectories (red, blue and green lines), fire detections by GOES (red dot symbols) and MODIS (green dot symbols) satellites, and NAAPS aerosol modeling of smoke, dust and sulfate, over a MODIS satellite image. The backward trajectories originate (red-cross symbols) from the aircraft flight path in the south Texas region. The red lines represent trajectories that began at different altitudes. The red lines represent trajectories that began at 100 m (328 ft), blue lines at 500 m (1640 ft), and green lines at 1000 m (3280 ft). *Source:* Image generated by 2008 TerraMetrics, Tele Atlas, Europa Technologies, Google Earth, and NASA.

The aircraft departed the Zapata County airport in the late afternoon (1:55 PM CDT) and flew within the CBL at approximately 305 m (1000 ft) MSL parallel to the Rio Grande River, i.e. U.S.-Mexico border (figure 16), to the Gulf of Mexico. At approximately 305 m (1000 ft) MSL near the Zapata area the wind direction was from

the southeast and closer to the Gulf of Mexico it was from the east-southeast (figure 16). The sky conditions were partly cloudy to clear (figure 15). Upon reaching the coast, the aircraft continued its flight path over the Gulf to a waypoint where it performed a vertical profile until above the CBL. After the vertical profile, the aircraft returned to the coast and flew more passes at different altitudes on the same flight path over the Gulf. Finally, the aircraft returned to the Zapata County airport parallel to the US-Mexico border within the CBL and performed another vertical profile near the Zapata County airport before landing.

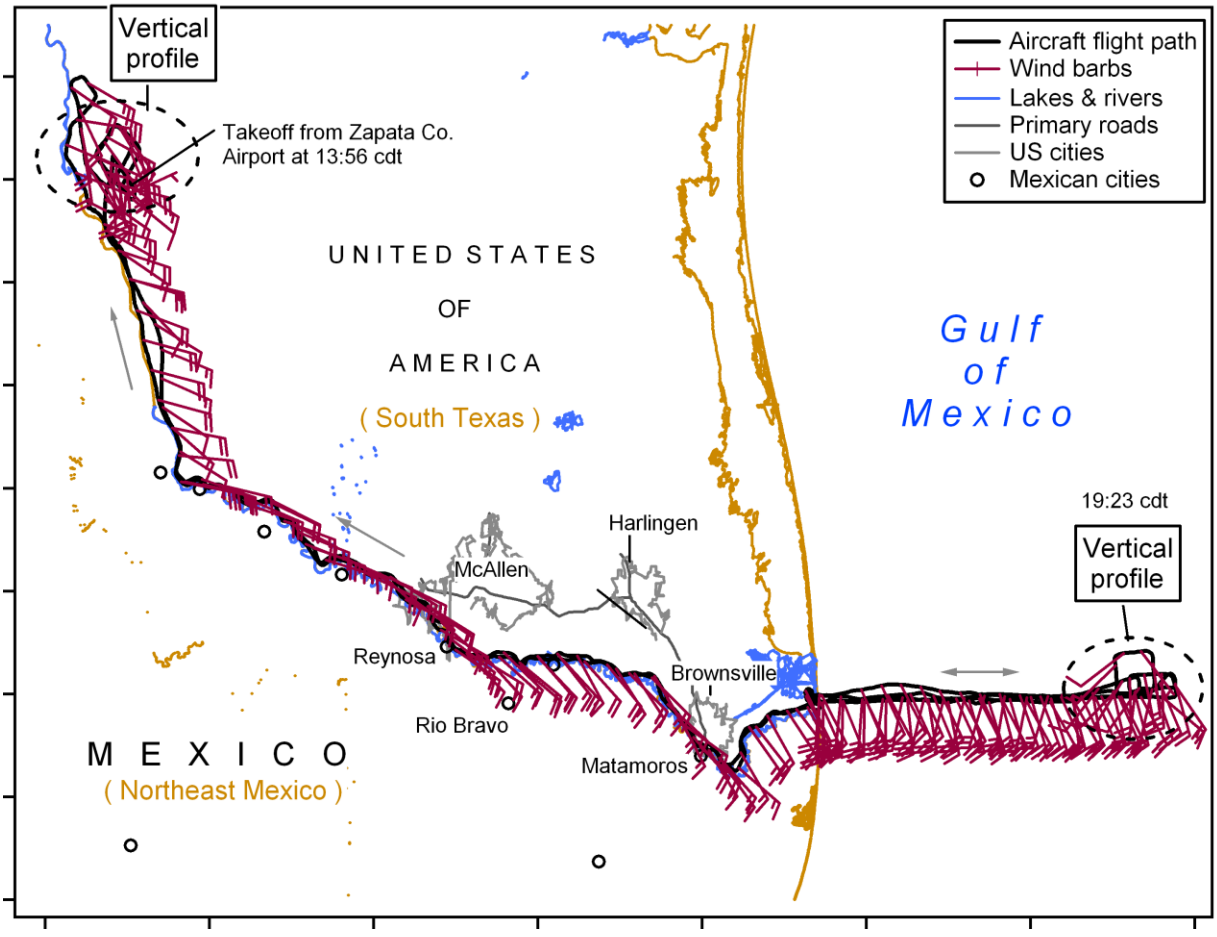

Figure 16. Map of aircraft path (black trace) and wind barbs. The black dashed circles are the approximate geographic locations where the vertical profiles were conducted.

Figure 17 and figure 18 illustrate atmospheric vertical profiles of trace gases and meteorological measurements. The plot on figure 17 (a) indicates elevated mixing ratios of CO over the Gulf and significant particle light scattering. Smoke was observed while flying over the Gulf with varying intensities. Figure 19 further illustrates a smoke plume over the western Gulf of Mexico with elevated CO mixing ratios above the marine layer and through the CBL.

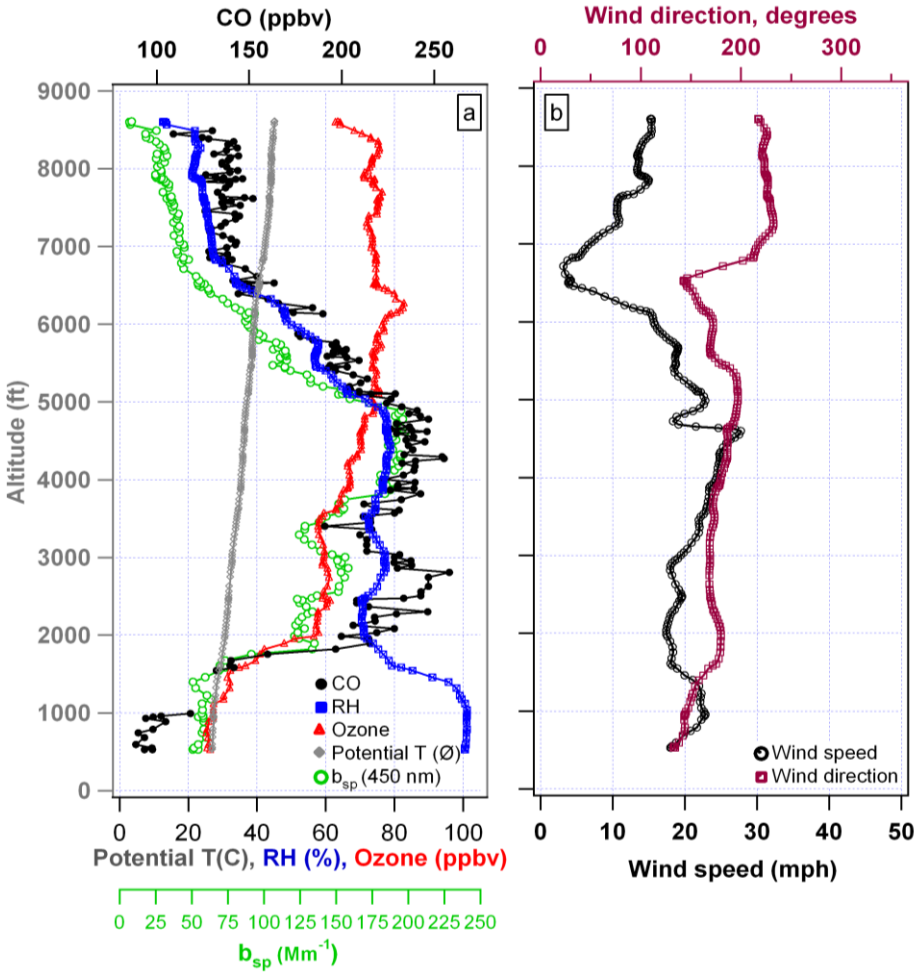

Figure 17. Panels (a) and (b) illustrate an atmospheric vertical profile flown on May 4, 2007 at 16:01 CDT from 213 to 2134 m (700 to 7000 ft) near the Gulf of Mexico. Panel (a) shows potential temperature, relative humidity, ozone, CO, and particle light scattering. Panel (b) displays wind speed and wind direction . Between 579 and 1829 m (1900 and 6000 ft), there is a well-pronounced increase in particle scattering and CO mixing ratios that suggest transported smoke from biomass burning in Mexico and Central America.

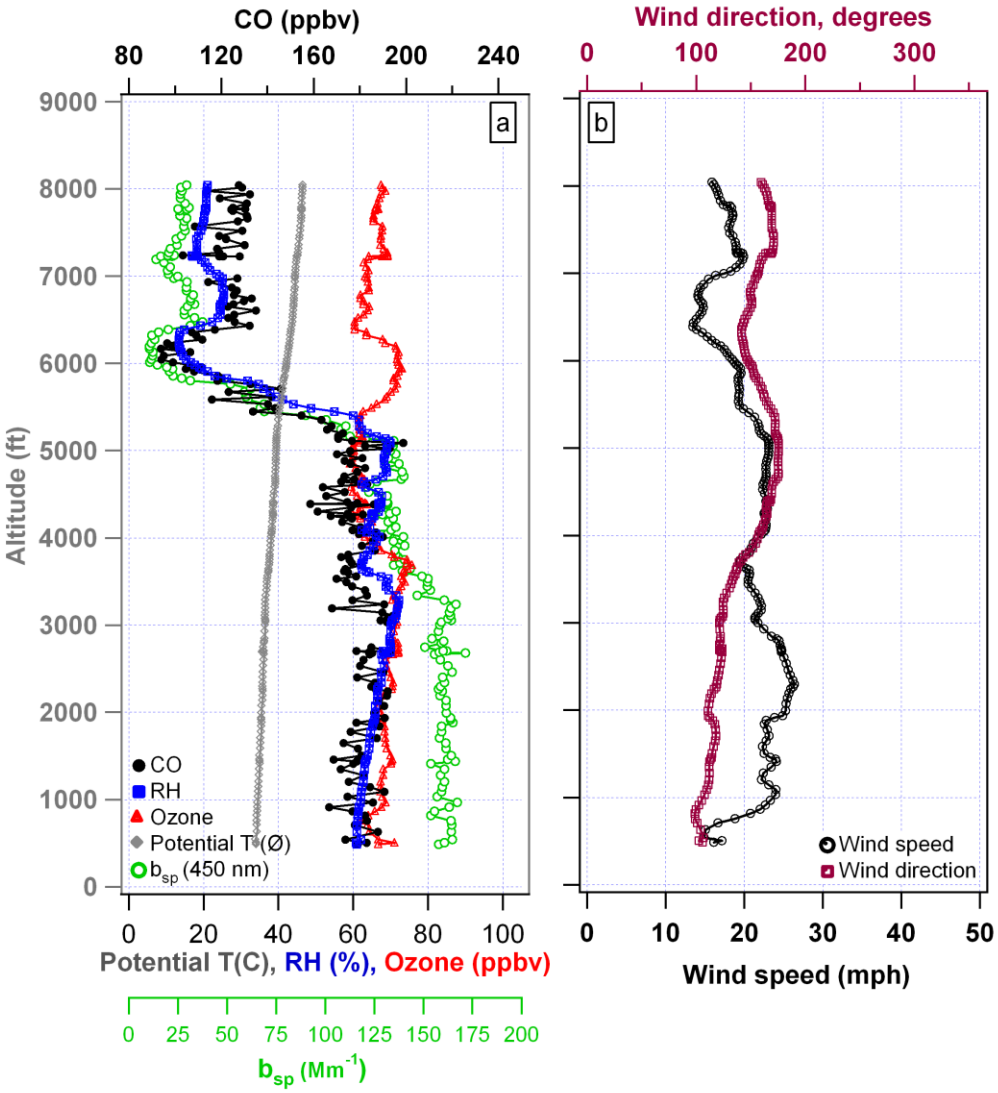

Figure 18 Panel (a) and (b) illustrate an atmospheric vertical profile flown on May 4, 2007 at 19:06 CDT from 154 to 2452 m (505 to 8046 ft) near the Zapata County airport (~115 mi or 185 km from the Gulf of Mexico). Panel (a) shows potential temperature, relative humidity, ozone, CO, and particle light scattering. Panel (b) displays wind speed and wind direction.

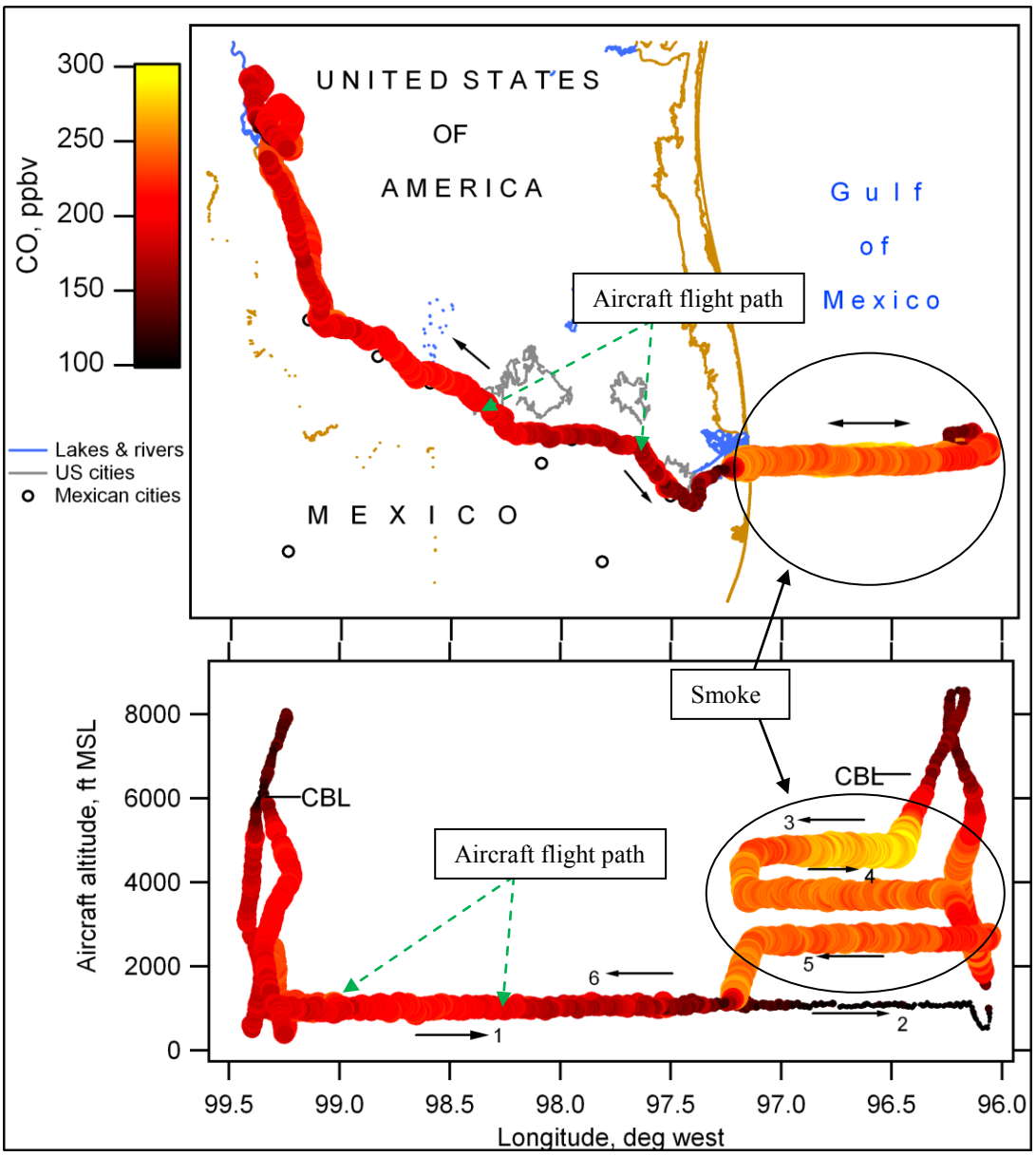

Figure 19. Aircraft flight path on May 4, 2007, color and symbol size color-coded by CO mixing ratio. The symbol size is proportional to CO mixing ratio.

Two aerosol filter samples (filters 01 and 06) were collected near the US-Mexico Border flight paths (i.e., within CBL) and four filters (filters 02, 03, 04, & 05) over the Gulf at different altitudes (see figure 19 and figure 20). Four VOC canisters were also sampled on this flight at different altitudes over the Gulf. Figure 20 indicates where the

VOC canister samples were collected and includes a table with the filter samples collected. The results of the VOC Canister and Aerosol Filter Samples are presented in table 3 and , respectively.

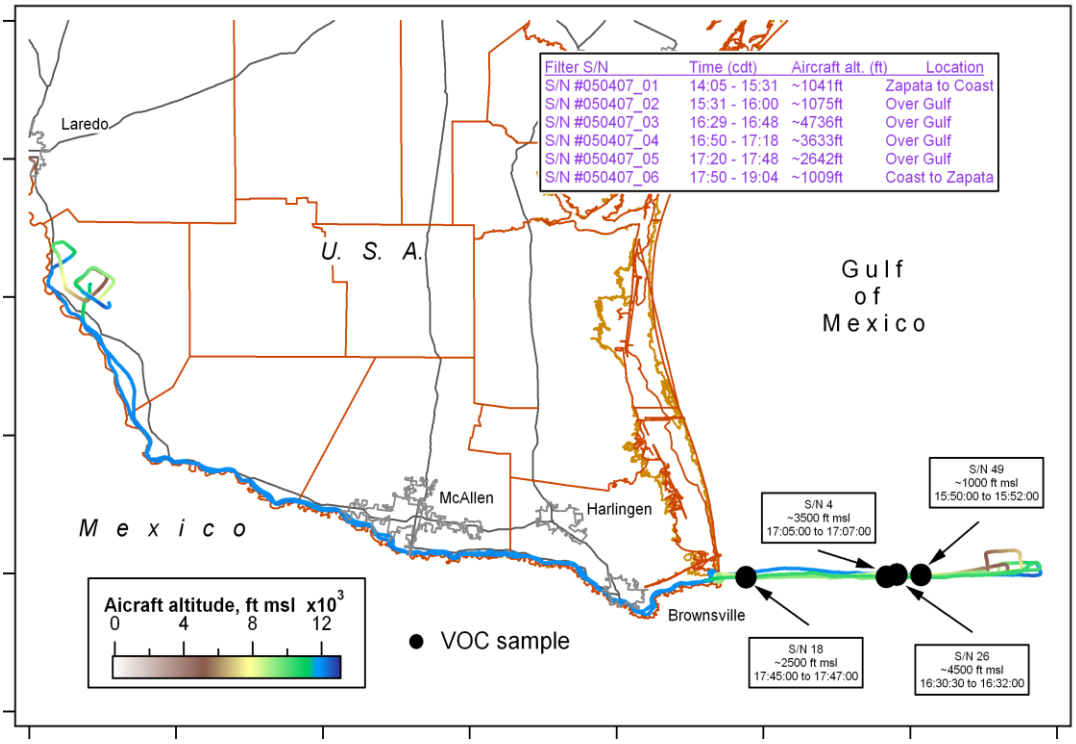

Figure 20. Map of aircraft flight path parallel to US-Mexico Border with color-coded aircraft altitude along flight path. VOC canister samples are indicated with black dot symbols on the flight path. The table on the upper right corner lists filters that were sampled during the flight.

The six aerosol filters showed a general gradient in the air mass composition primarily as a function of altitude. Near the surface (~ 1000 ft or ~305 m) cleaner air was sampled inland for the first and the last sample relative to the other samples. Both filters were exposed to aerosols of marine layer and continental air origin between Zapata and the coast. Biomass burning impacted air was intercepted to varying degrees in the four filters collected over the Gulf of Mexico. These four Gulf of Mexico filters samples were collected sequentially from 335 m (1100 ft), 1433 m (4700 ft), 1097 m (3600 ft), and then

797 m (2600 ft). All the Gulf of Mexico filters demonstrated biomass burning influence (i.e., elevated $C_2O_4^{-2}$ and K^+) with the lowest altitude filter (02) having a minor burning influence and a major sea-salt signal (i.e., elevated Na^+ and Cl^- ion concentrations). The sample from 4700 ft was not as impacted as the air mass sampled between 610 m (2000 ft) and 1219 (4000 ft). The back trajectories support this finding with the lower level trajectories originating in northeastern Mexico (an area with considerable burning at this time) and higher trajectories indicating an air mass originating in northwestern Mexico (figure 14).

Table 3. Aerosol Filter Analysis and Other Aircraft Data Averaged Over Filter Exposure Time Periods for 04 May 2007 Flight. (Aerosol filter data courtesy University of New Hampshire).

Sample ID	050407_01	050407_02	050407_03	050407_04	050407_05	050407_06
Altitude (ft)	1041	1075	4737	3634	2643	1010
Start-time (LST)	14:05	15:31	16:29	16:50	17:20	17:50
Stop-time (LST)	15:31	16:00	16:48	17:18	17:48	19:04
Total volume sampled (L)	8600	2900	1754	2800	2800	7400
Na^+ (pptv)	748	3054	1051	597	1074	439
NH_4^+ (pptv)	1403	15343	127	4623	5162	1962
K^+ (pptv)	122	828	167	313	326	178
Mg^{2+} (pptv)	85	374	42	67	76	31
Ca^{2+} (pptv)	311	2299	192	238	114	66
Cl^- (pptv)	315	1218	671	215	243	207
NO_3^- (pptv)	321	1136	49	239	347	111
SO_4^{2-} (pptv)	727	7947	80	2355	2624	1099
$C_2O_4^{-2}$ (pptv)	80	699	13	168	206	79

Table 3, continued

Sample ID	050407_01	050407_02	050407_03	050407_04	050407_05	050407_06
O_3 (ppbv)	52	30	77	62	60	51
NO (ppbv)	0.1	0.1	0.2	0.0	0.0	0.0
NO_2 (ppbv)	1.2	0.5	0.5	0.5	0.5	1.4
NOy (ppbv)	2.3	0.8	2.8	2.0	2.0	2.6
CO (ppbv)	186	103	253	236	230	178
SO_2 (ppbv)	0.3	0.2	0.5	1.0	1.0	0.3
Aerosol Backscatter @ 400 nm (Mm^{-1})	158	57	173	178	167	157
Air Temp (deg C)	29	25	22	23	25	29
RH (%)	76	94	71	86	76	77
WD (deg)	130	155	190	169	155	121
WS (mph)	17	23	30	24	22	22

Table 4 lists the analyses of three canisters (#49, #26, and #4) that were sampled from the same general geographical region over the Gulf of Mexico, whereas canister #18 was sampled just off the coast while the aircraft was heading back towards inland. Wind flows during sampling were southeast to south. Sampling over the Gulf allows the analysis of air masses which are presumably least impacted by immediate anthropogenic emissions. In fact, canister sample #49 taken at 1000 ft (305 m) reflected almost unpolluted marine air. All of the measured species showed low values during canister samplings. For instance, NO_x was about 0.2 ppb, CO about 100 ppb, and O_3 about 29 ppb, which are typical values for background conditions in the Gulf of Mexico. Particle light scattering showed minimum values. The total hydrocarbon burden was 15.3 ppbC. Mixing ratios of longer lived alkanes and acetylene (a typical combustion tracer) were low.

Table 4. VOC Canister Analyses (VOC data courtesy of University of Houston)

mixing ratios [pptv]	Can S/N 49	Can S/N 26	Can S/N 04	Can S/N 18
ethane	361	1971	3812	1969
ethylene	445	193	1628	252
propane	65	608	1083	415
propylene	230	35	1211	46
i-butane	65	56	90	52
n-butane	23	153	296	91
acetylene	90	483	494	419
t-2-butene	32	13	36	b.d.l.
1-butene	43	b.d.l.	370	11
i-butene	189	51	159	70
c-2-butene	22	14	58	b.d.l.
cyc-pentane	11	13	b.d.l.	10
i-pentane	61	64	96	74
n-pentane	26	40	82	32
1,3-butadiene	14	b.d.l.	37	b.d.l.
cyc-pentene+2-me-2-butene	b.d.l.	b.d.l.	37	b.d.l.
t-2-pentene	20	b.d.l.	18	b.d.l.
2-me-1-butene	41	b.d.l.	33	b.d.l.
1-pentene	20	b.d.l.	85	b.d.l.
3-me-1-butene	b.d.l.	b.d.l.	b.d.l.	b.d.l.
c-2-pentene	b.d.l.	b.d.l.	16	b.d.l.
2,2-dime-butane	b.d.l.	b.d.l.	b.d.l.	b.d.l.
2,3-dime-butane	b.d.l.	b.d.l.	b.d.l.	b.d.l.
2-me-pentane	b.d.l.	b.d.l.	14	b.d.l.
3-me-pentane	b.d.l.	b.d.l.	b.d.l.	b.d.l.
isoprene	25	b.d.l.	15	17
n-hexane	b.d.l.	11	15	13
c-3-hexene	b.d.l.	b.d.l.	b.d.l.	b.d.l.
t-2-hexene	14	b.d.l.	11	b.d.l.
c-2-hexene	b.d.l.	b.d.l.	11	11
me-cyc-pentane	b.d.l.	b.d.l.	b.d.l.	b.d.l.
2,4-dime-pentane	20	18	19	18
benzene	24	121	107	110
cyc-hexane	b.d.l.	b.d.l.	b.d.l.	b.d.l.
2-me-hexane	b.d.l.	b.d.l.	b.d.l.	b.d.l.
2,3-dime-pentane	74	76	73	54
3-me-hexane	28	b.d.l.	b.d.l.	b.d.l.
2,2,4-trime-pentane+1-heptene	300	256	255	170
n-heptane	6	b.d.l.	b.d.l.	b.d.l.
2,3-dime-2-pentene	15	b.d.l.	23	22
me-cyc-hexane	b.d.l.	b.d.l.	b.d.l.	9
2,3,4-trime-pentane	230	193	185	148
toluene	607	563	591	482
2-me-heptane	12	b.d.l.	b.d.l.	6
4-me-heptane	b.d.l.	b.d.l.	b.d.l.	b.d.l.
3-me-heptane	b.d.l.	b.d.l.	b.d.l.	b.d.l.
n-octane	b.d.l.	b.d.l.	b.d.l.	b.d.l.
et-benzene	b.d.l.	b.d.l.	9	b.d.l.
m,p-xylene	6	b.d.l.	b.d.l.	11
styrene	27	b.d.l.	b.d.l.	b.d.l.
o-xylene	12	b.d.l.	b.d.l.	b.d.l.
n-nonane	25	b.d.l.	b.d.l.	b.d.l.
i-prop-benzene	6	b.d.l.	b.d.l.	b.d.l.
n-prop-benzene	b.d.l.	b.d.l.	b.d.l.	9
m-et-toluene	b.d.l.	b.d.l.	b.d.l.	b.d.l.
1,3,5-trime-benzene	b.d.l.	b.d.l.	b.d.l.	b.d.l.
o-et-toluene	b.d.l.	b.d.l.	b.d.l.	27

Light alkenes (ethylene, propylene) were slightly enhanced possibly due to some marine biogenic emissions which also depend on wind conditions. Between canisters #26 and #4, canister #26 showed the higher hydrocarbon burden (34.3 ppbC) and showed distinctly elevated values for reactive alkenes: ethylene, 1.6 ppbv; propylene, 1.1 ppbv, as well as combustion related acetylene. This layer seemed to contain the highest reactive NMHC pool. The other canisters (#26 and #18) already reflected partially photochemically processed air with lower amounts of short lived NMHCs. However, the acetylene fraction was still considerable (about 5% of the entire hydrocarbon burden expressed as [ppbC]). This is a strong indication that these air masses were impacted by combustion processes. Thus, it is very likely that the layer between 1800-5000 ft over the Gulf of Mexico shown in figure 17 and figure 19, contained levels of smoke. Given the predominant east to southeast wind flows during this time, it is likely that the vertical profile shown in figure 18 was also impacted by smoke. Although the upper limit of this layer was around 5000 ft, it seems that the plume was able to reach the surface, most likely due to enhanced vertical mixing over the continental areas during daytime, a process that does not readily occur over ocean surfaces.

CHAPTER FOUR

Conclusions and Recommendations

The results from analyzing two science flights has added to the knowledge of the details of the air quality in the Rio Grande Valley region and the broader Rioplex region during the spring season, April to May, when southeasterly synoptic flow occur and transboundary transport of primary and secondary pollutants, in particular related to biomass burning during the dry season, are likely.

The Baylor Institute for Air Science (BIAS) equipped an aircraft to measure the air composition during two science flights in the area south Texas region. One science flight was flown to collect "background" continental and marine layer air data and the other to collect data in biomass-burning smoke plumes from Mexico and Central American countries. Measurements were taken in the geographic region along the US-Mexico Border and adjacent area over the western Gulf of Mexico. Flight patterns were based on the probability that smoke would be transported over the region as predicted by characteristic meteorological patterns.

Results of this study indicate that individual smoke plumes may occur episodically over the Texas border region to Mexico under prevailing southeasterly wind directions. The origin of these plumes may be diverse including smoke plumes from individual local fire emissions (i.e., RioPlex), medium range transport from northeast and central Mexico and long range from Yucatan, southern Mexico and Central American

countries. Though airborne measurements were only able to observe smoke plumes confined to specific layers aloft, it cannot be ruled out that these air masses eventually will mix into the lower layers and reach the surface, if not immediately along the Texas border region to Mexico, potentially in other areas further downwind. Thus, they may contribute to enhance the aerosol mass loading and surface ozone concentration. Depending on the duration of these events, these plumes may contribute to a NAAQS particulate matter (2.5 and 10 micron) or ozone standard.. This effect may be of significant magnitude if these plumes still contain sufficient reactive hydrocarbons and aerosols, and eventually mix with air masses exposed to higher than background NO_x emissions, e.g. in urbanized areas. Smoke plumes can be identified as enhancements of CO, K^+ and $C_2O_4^{-2}$ ions, but cannot be fully described due to the lack of sufficiently accurate emission inventory for the Mexico domain and Central American countries.

Because the study was limited to one spring season, variations from one year to another may be large, but unfortunately could not be considered due to project time constraints. However, such study may be desirable, since this particular study was only able to capture individual small scale plumes with chemical markers. Large scale plumes may be present in other years and lead to regional impacts, even throughout the state of Texas, which potentially would have an additional adverse impact on air quality in regions like the Houston-Galveston area and may need to be considered in local air quality forecasts.

Any long term changes with data from these two science flights could not be addressed in this limited study. Future work is recommended in the evaluation of

additional data from these two flights of O_3, NO_x, NO_y, particle size distributions, and particle light scattering. Additionally, it is recommended to analyze other science flights that were flown during the 2007 biomass burning season. Enhancing the existing ground monitoring sites in Zapata County, the Rio Grande Valley and Mexico with ion speciation, SO_2, NO_x, NO_y and CO is recommended. Finally, it is recommended that additional ground monitoring sites are sited on south side and north side of the Rioplex area to address transboundary pollution in both the United States and Mexico. These kind of efforts can be accompanied by airborne measurements on a campaign basis during selected times of the biomass burning season to sample and characterize the biomass burning plumes aloft in terms of physical and chemical properties, to evaluate their extension, their origin and their pathways into larger areas in Texas.

REFERENCES

Alvarez, S., Compton, T., Shauck, M., Zanin, G., Rappenglück, B., Lefer, B., Byun, Daewon. (2008). Airborne air quality sample collection in Zapata County (MexCAmTex) during the 2007 biomass burning season, Report submitted to Zapata County USEPA project grant, p 8-142.

Andreae, M. O. (1991). Biomass burning: Its history, use and distribution and its impact on environmental quality and global climate, in Global Biomass Burning, edited by J.S. Levine, 3-21, MIT Press, Cambridge.

Brain, C. K. & Sillen, A. (1988). Evidence from the Swartkrans cave for the use of fire. *Nature*, 336, 464-466. doi:10.1038/336464a0

Crutzen, P. J. & Andreae, M. O. (1990). Biomass burning in the tropics: impact on atmospheric chemistry and biogeochemical cycles. *Science,* 250, 1669-1678.

Crutzen, P. J., Heidt, J. P., Krasnec, W. H., Pollock, W. H., Seiler, W. (1979). Biomass burning as a source of atmospheric gases CO, H_2, N_2O, NO, CH_3Cl, and COS. *Nature*, 282, 253-256.

de Gouw, J. A., Warneke, C., Parrish, D. D., Holloway, J. S., Trainer, M., Fehsenfeld, F. C. (2003). Emission sources and ocean uptake of acetonitrile (CH3CN) in the atmosphere. *Journal of Geophysical Research*, 108, 4329. doi:10.1029/2002JD002897

Dickerson, R. R., Kondragunta S., Stenchikov G., K. L. Civerolo K. L., Doddridge B. G., & Holben N. (1997). The impact of aerosols on solar ultraviolet radiation and photochemical smog, *Science*, 278, 827–830.

Draxler, R. R. & Rolph, G.D. (2003). HYSPLIT (HYbrid Single-Particle Lagrangian Integrated Trajectory) Model access via NOAA ARL READY Website (http://www.arl.noaa.gov/ready/hysplit4.html). NOAA Air Resources Laboratory, Silver Spring, MD.

Dwyer, E., Pinock, S., Grégoire, J. M., & Pereira, M. C. (2000). Global spatial and temporal distribution of vegetation fire as determined from satellite observations. *International Journal of Remote Sensing*, 21, 6 & 7, 1289-1302.

Dwyer,.E., Grégoire, J. M. , & Lalingeau. (1998). A global analysis of vegetation fires using satellite images: Spatial and temporal dynamics. *Ambio*, 27, 175-181.

Fearnside, P. M., (1990). Fire in the tropical rain forests of the Amazon Basin, in Fire in the Tropical Biota. *Ecological Studies*, 48. edited by J. G. Goldammer, 106-115. New York, Springer-Verlag.

Gebhart, K. A., Kreidenweis, S. M., Malm, W.C. (2001). Back-trajectory analyses of fine particulate matter measured at Big Bend National Park in the historical database and the 1996 Scoping study. *Science Total Environment*, 36, 185-204.

Hsu, N., Herman, J., Bharitia, P., Seftor, C., Torres, O., Thompson, A., Gleason, J., Eck, T., Holben, B. (1996). Detection of biomass burning smoke from TOMS measurements. *Geophysical Research Letters*, 23, 745-748.

Hutchison, K. D. (2003). Application of MODIS satellite data and products for monitoring air quality in the state of Texas. *Atmospheric Environment*, 37, 2403-2412.

INDEGI. (2005). Instituto Nacional De Estadística y Geografía. Conteo de población y vivienda 2005 Estados Unidos Mexicanos: Síntesis de resultados. Retrieved March 1, 2009, from INDEGI, http://www.inegi.org.mx/inegi/default.aspx?s=est&c=10419&pred=1

Jacobson, M. Z. (1998). Studying the effects of aerosols on vertical photolysis rate coefficient and temperature profiles over an urban airshed, *Journal of Geophysical Research.,* 103(D9), 10,593– 10,604.

Kreidenweis, S. M., Remer, L. A., Bruintjes, R., Dubovik, O., Smoke aerosol from biomass burning in Mexico. *Journal of Geophysical Research*, 106, 4831-4844.

Levine, J. S. (1996). Biomass burning and global change: Remote sensing and modeling of biomass, and biomass burning in the boreal forest. Cambridge: MIT Press.

Leuchner, M., & Ruppenglück, B. (2009). VOC source-receptor relationships in Houston during TexAQS-II, *Atmospheric Environment*, doi:10.1016/j.atmosen v.2009.02.029

Lobert, J. M, William, K. C., Logan, J. A, & Yevich, R. (1999). Global chlorine emissions from biomass burning: Reactive Chlorine Emissions Inventory. *Journal of Geophysical Research,* 114(D7). 8373-8389. doi:10.1029/2005JD006319

McAllen Chamber of Commerce. (2008). McAllen Chamber Economic Profile. Retrieved February 23, 2009, from McAllen Chamber of Commerce, http://www.mcallen.org/pdf/profile/McAllenOverview2008.pdf

Mendoza, A., Garcia, M. R., Vela, P., Lozano, F. & Allen, D. (2005, December). Trace gases and particulates matter emissions from wildfires and agricultural burning in northeastern Mexico during the 2000 fire season. *Journal of Air & Waste Management Association,* 55, 1797-1808.

NOAA. (2006). *Smoke Forecast Verification Using Hazard Mapping Sysytem, NESDIS Text Narrative*. Retrieved April 22, 2007 and May 4, 2007, from NOAA Smoke Forecasting System: http://www.ready.noaa.gov/smoke/verifyhms.html

Peppler, R. A., Bahrmann, C. P., Barnard, J. C., Campbell, J. R., Cheng, M. D., Ferrare, R. A., Halthorne., R. N., Heilman. L. A., Hlavka, D. L., Laulainen, N. S., Lin, C. J., Ogren, J. A., Poellot, M. R., Remer, L. A., Sassen, K., Spinhirne, J. D., Splitt, M. E., Turner, D. D. (2000). Arm southern Great Plains site observations of the smoke associated with the 1998 Central AmericanFires. *Bulletin of the American Meteorological* Society, 81, 2563-2591.

Rokjin, J., Jacob, J. J., & Logan, J. A. (2007). Fire and biofuel contributions to annual mean aerosol mass concentration in the United States. *Atmospheric Environment*, 41, 7389-7400.

Rolph, G.D. (2003). Real-time Environmental Applications and Display sYstem (READY) Website (http://www.arl.noaa.gov/ready/hysplit4.html). NOAA Air Resources Laboratory, Silver Spring, MD.

Rappenglück B., Apel E., Bauerfeind M., Bottenheim J., Brickell P., Čavolka P., Cech J., Gatti L., Hakola H., Honzak J., Junek R., Martin D., Noone C., Plass-Dülmer Ch., Travers D., Wang T (2006): The first VOC intercalibration exercise within the Global Atmosphere Watch (GAW), *Atmospheric Environment*, 40, 7508-7527, doi:10.1016/j.atmosenv.2006.07.016

Simoneit, B. R. T., Schauer, J. J., Nolte, C.G., Oros, D. R., Elias, V. O., Fraser, M. P., Rogge, W. F., Cass. G. R. (1999). Levoglucosan, a tracer for cellulose in biomass burning and atmospheric particles, *Atmospheric Environment*, 33, 173-182.

Trentmann, J. (2001). Atmospheric processes in a young biomass burning plume (Doctoral dissertation zur Erlangung des Doktogrades der Naturwissenschaften der Universität Hamburg, 2001).

Veillerot M., Locoge N., Galloo J.C., Guillermo R. (1998): Multidimensional capillary gas chromatography for the monitoring of individual non-methane hydrocarbons in air, *Analusis Magazine*, 26, M38-M43

Wang, J., Christopher, S. A., Nair, U. S., Reid, J. S., Prins, E. M., Szykman, J., Hand, J. L. (2006). 1. Mesoscale modeling of Central American smoke transport to the United States: "Top-down" assessment of emission strength and diurnal variation impacts. *Journal of Geophysical Research*, 111, D05S17, doi:10.1029/2008JD010807

Westerling, A. L., Hidalgo, H. G., Cayan, D. R., Swetnam, T.W. (2006). Warming and earlier spring increases western US forest wildfire activity. *Science*, 319, 940-943.

Wikipedia: the free encyclopedia. (2004, July 22). FL: Wikipedia Foundation, Inc. Retrieved February 23, 2009, from http://www.wikipedia.org